Hierarchical Curl-Conforming Vector Bases for Pyramid Cells

Roberto D. Graglia⬢, *Life Fellow, IEEE*, and Paolo Petrini⬢, *Member, IEEE*

Abstract—**Advanced applications of the finite-element method use hybrid meshes of differently shaped elements that need transition cells between quadrilateral- and triangular-faced elements. The greatest ease of construction is obtained when, in addition to triangular prisms, one uses also pyramids with a quadrilateral base, as these are the transition elements with the fewest possible faces and edges. A distinctive geometric feature of the pyramid is that its vertex is the point in common with four of its faces, while the other canonical elements have vertices in common with three edges and three faces, and that is why pyramids' vector bases have hitherto been obtained with complex procedures. Here, we present a much simpler and more straightforward procedure by shifting to a new paradigm that requires mapping the pyramidal cell into a cube and then directly enforcing the conformity of the vector bases with those used on adjacent differently shaped cells (tetrahedra, hexahedra, and triangular prisms). The hierarchical curl-conforming vector bases derived here have simple and easy to implement mathematical expressions, including those of their curls. Base completeness is demonstrated for the first time, and results confirming the avoidance of spurious modes and faster convergence are also reported.**

Index Terms—**Electromagnetic fields, finite-element methods, higher order vector elements, numerical analysis, pyramidal elements.**

I. Introduction

VERY accurate 3-D models that balance computational efficiency with geometric flexibility are obtained using the hybrid meshes of tetrahedra, hexahedra (bricks), and prismatic cells together with interpolatory [1], [2] or hierarchical vector bases [3]–[5] of high order. All these divergence- and curl-conforming bases are now reported in a single book [6]. Curl-conforming bases with continuous tangential components across adjacent cells in the mesh are used in finite-element method (FEM) applications to discretize the vector Helmholtz operator. Hierarchical bases are preferred in applications that implement *p*-adaptive refinement techniques, because they easily allow for a selective expansion using a different order in different regions of the computational domain, which often leads to reduced computation time and more accurate results [7]–[9]. It is difficult to create conforming hybrid

meshes without pyramid elements. (The definition of the conforming mesh is given, for example, in [6, Ch. 2].) Pyramids with a quadrilateral and four triangular faces are in fact the most obvious natural *fillers* for discretizations mostly formed by other differently shaped cells. For example, pyramids are required when one has to link a coarse to a dense mesh of bricks (see [10, Fig. 2] and [11, Fig. 1]).

This article presents the pyramid's bases that conform to and complete the hierarchical curl-conforming families reported in [6]. Our new basis functions are obtained directly, simply by multiplying the lowest order vector functions given in [11] by a suitable set of generating *scalar polynomials*, thereby using, in essence, the same technique already used in [3]–[6] to obtain the bases for the other 3-D elements. More importantly, this article provides ready-to-use expressions of the vector basis functions, normalized to obtain relatively low mass-matrix condition numbers (CN) in FEM applications.

As with the other hierarchical volumetric elements in [6], our new pyramid bases have four distinctive features: 1) the vector basis functions are subdivided from the outset into three different groups of edge-, face-, and volume-based functions; 2) each basis function is obtained by using one *generating* edge-, face-, or volume-based *scalar* polynomial whose analytical expression involves all the dependent variables that describe the cell; 3) the generating polynomials are either symmetric or antisymmetric with respect to the variables that describe each edge and face of the cell, and are organized hierarchically; and 4) in each group, the generating polynomials are mutually orthogonal for inner product defined by the integral on the volume, the face, or the edge of the cell.

To put our work in perspective, note that in the late 1990s, practitioners were satisfied with using pyramidal bases at most of the first order [11]–[13], as it was not clear the number of volume-based functions needed for higher orders. Research in this area has then received a new impetus from 2010 onward, with important results published mainly in applied mathematics journals (see [14]–[18] and references therein). Unfortunately, the specialized literature has privileged theoretical aspects so that it is difficult to extract from this literature ready-to-use recipes for computational applications. In fact, until now, the use of higher order pyramid bases has been hampered by the complex procedures used to generate them. Also, as discussed in this article, in the volume, inside the pyramid, the vector basis functions have a fractional form that is more complicated than that proposed in [11], as it became apparent in other papers [13], [15]–[18] published after [11]. Indeed, as noted in [19], for orders higher than the first, the bases in [11] lead to spurious modes, because they are

constructed with multiplicative polynomials of the parent variables that vary linearly in the so-called *parent* pyramidal cell. The correct multiplicative functions are obtained here by working in a different space of *scaled* parent variables, which we call the *grandparent* space, where the pyramidal cell is mapped by a cube on which we compute the FEM volume integrals; in the grandparent cube, the vector basis functions and their curl, as well as the multiplicative functions and their gradient, all have polynomial form.

Although the bases in [11] can yield spurious modes, they are complete in their space and, on the pyramid boundary, they can take the same "polynomial" expression as those of differently shaped elements. This has prompted us to *reverse* the derivation technique adopted elsewhere [17], as the edge- and face-based functions reported here have been derived starting from the known expression of the functions of adjacent, differently shaped elements (so to speak, by imposing a tangential continuity at the boundary of the cell), while the volume-based functions are obtained thanks to simple analytical and geometric considerations. Our volume-based functions differ from those given in [16] and [17]; their order does not exceed that of the edge- and face-based vector functions whose number and order are dictated by continuity with adjacent elements. In our opinion, this amounts to saying that the main problem that researchers have had up to now to build the pyramid's bases is to find the simplest and most direct way to build the volume-based vector functions, and then prove the completeness of the whole family which, to the best of our knowledge, is given here for the first time in the Appendix. The proof in the Appendix shows that a complete vector base is obtained using multiplicative scalar functions of the grandparent domain of well-determined maximum polynomial order.

The rest of this article is structured as follows. In Section II, we explain why the basis functions and their curls shall belong to a common (polynomial) subspace to be identified from the outset. Section III describes the geometric representation of the pyramidal element, while the variables used to define the polynomial bases are discussed at length in Section IV, which also reports the lowest order base. The higher order bases are given in Section V, while numerical results are reported in Section VI. Readers may find it useful to review [11] for a detailed introduction to the notation and other background information, as well as the fundamental paper [17] that inspired ours.

II. BASIS FUNCTIONS' SUBSPACES

Polynomial vector bases accompany tetrahedral, brick, and prismatic cells in a completely natural way, because only three edges and three faces branch off from the vertices of a tetrahedron, a brick, and a triangular prism. Conversely, since the pyramid has four edges and faces converging at one vertex, it is necessary to explain why to look for polynomial bases for the pyramid as well. In this regard, we observe that FEM problems are usually formulated in terms of a single main unknown: either the magnetic field H or the electric field E. The other field is determined by the curl of the main field, as imposed by one of the Maxwell's curl equations. For example, to clarify, the electromagnetic fields that can

exist within a 3-D cavity formed by perfectly conducting walls, containing homogeneous or inhomogeneous dielectric and magnetic materials, may be found by solving one of the following vector Helmholtz equations [6]

$$\nabla \times \left(\frac{1}{\epsilon_r} \nabla \times H \right) - k^2 \mu_r H = 0 \tag{1}$$

$$\nabla \times \left(\frac{1}{\mu_r} \nabla \times E \right) - k^2 \epsilon_r E = 0 \tag{2}$$

where $\epsilon_r(x, y, z)$ and $\mu_r(x, y, z)$ denote the relative permittivity and relative permeability functions, respectively. (Section VI reports some results for pyramid-shaped cavities obtained by solving Helmholtz's equation numerically.) FEM formulations in terms of H or E do not show significant differences except for the different way used to impose the boundary conditions. In fact, curl-conforming bases are derived with no reference to the main field we want to represent, since E and H swap in the dual problem. In all 3-D FEM applications, the curl-conforming basis functions Ω are expressed in the most convenient way, i.e., using three coordinate gradient vectors $\nabla \xi_a$, $\nabla \xi_b$, and $\nabla \xi_c$ (which are curl-free); the curl of the basis functions can then be expressed in terms of unitary basis vectors ℓ^a, ℓ^b, and ℓ^c (see [1] and [6] and Section III). Thus, for the pyramid, we may write

$$\Omega = A_a \nabla \xi_a + A_b \nabla \xi_b + A_c \nabla \xi_c \tag{3}$$

$$\nabla \times \Omega = \frac{1}{\mathcal{J}} \left(B_a \, \ell^a + B_b \, \ell^b + B_c \, \ell^c \right) \tag{4}$$

where A_i and B_i turn out to be nonpolynomial functions of the parent variables. Without specifying the subspace to which they belong, here we can only require that (3) and (4) are finite-energy functions. Of course, this is too little, since H and E are interchangeable and constrained by Maxwell's curl equations, and especially because we may wish to rewrite Ω in terms of the unitary basis vectors. It is therefore reasonable to expect and require that vector basis functions and their curls belong to a much better specified *common* subspace, perhaps a polynomial one, as it happens for all the other elements.

Since we know the lowest order pyramidal basis functions from [11], in Section IV, we easily identify the polynomial subspace in common to the basis functions and their curls. There, we see that the coefficients A_i and B_i in (3) and (4) are polynomials of variables other than the parent ones, although related to them. The higher order volume-based vector functions are obtained by inspection once we understand which variables we must use to get vector bases of polynomial form.

III. ELEMENT GEOMETRY REPRESENTATION IN CHILD AND PARENT SPACE

With reference to Fig. 1, any *child* pyramid in the observer's space $r = (x, y, z)$ is a mapping of the same *parent* pyramid obtained through the *shape functions* of five parent variables $\xi = (\xi_1, \xi_3; \xi_2, \xi_4; \xi_5)$ that vary linearly across the element. The faces are numbered to correspond to the indexing of the associated parametric coordinates; that is, the j-th face of the pyramid lies on the parametric surface $\xi_j = 0$. The quadrilateral face lies on the coordinate surface $\xi_5 = 0$, while
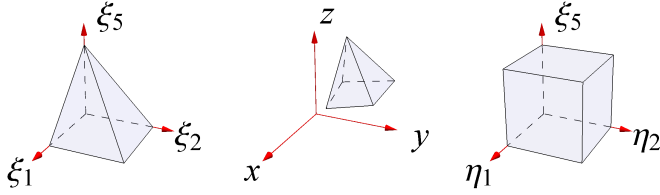
Fig. 1. Shape functions map the parent pyramid in the left to the child pyramid in the center. In the grandparent space $(\boldsymbol{\eta}, \xi_5)$, the shape functions and the basis functions take polynomial form, while the pyramid is described by the cubic cell shown in the right.

the four triangular faces have coordinate $\xi_j = 0$, with $j = 1$ to 4. We choose as *independent* coordinates ξ_1, ξ_2, and ξ_5, so that $\nabla \xi_5 \cdot (\nabla \xi_1 \times \nabla \xi_2)$ is strictly positive (see Fig. 1), while ξ_3 and ξ_4 are *dependent* coordinates. Gradient $(\nabla \xi_a)$ and edge $(\boldsymbol{\ell}_{ab})$ vectors are defined in the child space and calculated as summarized in Table I. Notice that the triangular faces 1 and 3 are opposite to each other and have in common only the vertex of the pyramid, as happens for faces 2 and 4. Henceforth, the subscripts that label the triangular faces are always computed modulo 4 meaning, for example, $\xi_{j-1} = \xi_4$ for $j = 1$, and $\xi_{\gamma+1} = \xi_1$ for $\gamma = 4$. Similarly, the edges are given a two-index label deriving from the two faces sharing the edge. The pyramid's edges shared by two triangular faces are called *triangle* edges to distinguish them from the *mixed* edges lying on the quadrilateral face and in common to only one triangular face; this naming is the same as used in [17]. The edges indicated by two dummy indices γ and $\gamma + 1$ are always triangle edges and, to lighten the notation, we will often set

$$\gamma + 1 = \delta. \tag{5}$$

The $\boldsymbol{\xi}$ variables are linked by the dependence relations [11]

$$\xi_1 + \xi_3 + \xi_5 = 1$$
$$\xi_2 + \xi_4 + \xi_5 = 1 \tag{6}$$

that hold also on each face of the cell. In fact, the parametric coordinates ξ_1, ξ_3, and ξ_5 used to describe the triangular face $\xi_2 = 0$ (as well as the $\xi_4 = 0$ face) are dependent on each other as in the first of (6). The coordinates ξ_2, ξ_4, and ξ_5 which describe the faces $\xi_1 = 0$ and $\xi_3 = 0$ are dependent on each other as in the second of (6). Finally, for the quadrilateral face $\xi_5 = 0$, one has the two dependency relations obtained from (6) by setting $\xi_5 = 0$. On the pyramid's tip, one has $\xi_5 = 1$, while (6) forces the remaining four coordinates to vanish.

IV. LOWEST ORDER BASIS FUNCTIONS AND NEW PARADIGM TO DERIVE HIGH-ORDER BASES

One of the main objectives of this section is to clarify which variables to use to get pyramidal bases of polynomial type, because certainly these bases are not of polynomial type if we specify them using the parent variables introduced in Section III. Thus, in addition to the parent coordinates, we introduce four *scaled* coordinates, for $j = 1, 2, 3, 4$

$$\eta_j = \frac{\xi_j}{1 - \xi_5} \tag{7}$$

$$\nabla \eta_j = \frac{\nabla \xi_j + \eta_j \nabla \xi_5}{1 - \xi_5} \tag{8}$$

with dependence relations (for $\xi_5 \neq 1$) stemming from (6)

$$\eta_1 + \eta_3 = 1; \quad \eta_2 + \eta_4 = 1. \tag{9}$$

These coordinates, used also in [17], transform surface integrals on the triangular face $\xi_j = 0$ of the parent pyramid (i.e., a triangular simplex) into integrals on a unit square, while volume integrals on the parent pyramid become integrals on the unit cube of the $(\boldsymbol{\eta}, \xi_5)$-space, as shown in (10) and (11)

$$\int_0^1 \int_0^{1-\xi_5} G(\xi_{j+1}, \xi_5) \, d\xi_{j+1} \, d\xi_5$$
$$= \int_0^1 \int_0^1 (1 - \xi_5) \, G[(1 - \xi_5)\eta_{j+1}, \, \xi_5] \, d\eta_{j+1} \, d\xi_5 \tag{10}$$

$$\int_0^1 \int_0^{1-\xi_5} \int_0^{1-\xi_5} G(\boldsymbol{\xi}) \, d\xi_1 \, d\xi_2 \, d\xi_5$$
$$= \int_0^1 \int_0^1 \int_0^1 (1 - \xi_5)^2 \, G(\boldsymbol{\eta}, \xi_5) \, d\eta_1 \, d\eta_2 \, d\xi_5. \tag{11}$$

The kernel on the right-hand side of (11) could be used to cancel singular terms that the function $G(\boldsymbol{\eta}, \xi_5)$ could have at the vertex of the pyramid, in $\xi_5 = 1$. For example, tip singularities could occur if the tip of the pyramid is an isolated vertex of the structure under consideration. To model physically permitted singularities, one should develop and use singular basis functions, which are beyond the scope of this article.

Most important of all is that the vector basis functions and their curl take a simple polynomial form in terms of the *grandparent* variables $(\boldsymbol{\eta}, \xi_5)$, as summarized in Table I, whereas they have a fractional form when using $\boldsymbol{\xi}$ parent variables [11]. The same happens to the shape functions; for example, the interpolatory shape functions used in [11] take a polynomial form by using (7) to replace the parent variables with the new grandparent ones.

In this regard, we immediately claim the fundamental result used to derive our bases which stems from (8), namely that the curl of any linear combination of terms such as $\eta_1^\alpha \eta_2^\beta \xi_5^z (1 - \xi_5) \nabla \xi_a$ (where the subscript a in $\nabla \xi_a$ is 1, 2, or 5), and the gradient of any linear combination of terms such as $\eta_1^\alpha \eta_2^\beta \xi_5^z (1 - \xi_5)$ takes a polynomial form in the space $(\boldsymbol{\eta}, \xi_5)$. (Of course, each term of these linear combinations can have different values of the exponents α, β, and z.)

With reference to Table I, the factor $(1 - \xi_5)^2$ guarantees the polynomial form to $\boldsymbol{\Omega}_{\gamma 5}$ and its curl, while the proof that the *polynomials* $\boldsymbol{\Omega}_{\gamma \delta}$ agree with the aforementioned fundamental result is obtained by highlighting their nonzero curl component

$$\boldsymbol{\Omega}_{\gamma \delta} = 2 \, \eta_{\gamma+2} \, \eta_{\delta+2} \, (1 - \xi_5) \, \nabla \xi_5 - \nabla \big[\eta_{\gamma+2} \, \eta_{\delta+2} \, \xi_5 \, (1 - \xi_5) \big] \tag{12}$$

which gives (for $\gamma = 1$ to 4, and $\delta = \gamma + 1$)

$$\nabla \times \boldsymbol{\Omega}_{\gamma \delta} = 2 \, \nabla \big[\eta_{\gamma+2} \, \eta_{\delta+2} \, (1 - \xi_5) \big] \times \nabla \xi_5$$
$$= -2 \, \big(\eta_{\gamma+2} \, \boldsymbol{\ell}_{\delta 5} + \eta_{\delta+2} \, \boldsymbol{\ell}_{\gamma 5} \big) / \mathcal{J}. \tag{13}$$

The curl-free *polynomial* vector on the right-hand side of (12) guarantees tangential continuity between adjacent elements and cannot be omitted. In fact, recall that the basis functions of Table I have a constant tangential (CT) component along each

TABLE I
PYRAMID'S GEOMETRY REPRESENTATION AND LOWEST ORDER CURL-CONFORMING BASE

The element Jacobian ($\mathcal{J}$) and the *gradient vectors* ($\boldsymbol{\nabla}\xi_a$)

$$\mathcal{J} = \boldsymbol{\ell}^1 \cdot \boldsymbol{\ell}^2 \times \boldsymbol{\ell}^5$$

$$\boldsymbol{\nabla}\xi_5 = \frac{\boldsymbol{\ell}^1 \times \boldsymbol{\ell}^2}{\mathcal{J}}, \quad \boldsymbol{\nabla}\xi_1 = \frac{\boldsymbol{\ell}^2 \times \boldsymbol{\ell}^5}{\mathcal{J}}, \quad \boldsymbol{\nabla}\xi_2 = \frac{\boldsymbol{\ell}^5 \times \boldsymbol{\ell}^1}{\mathcal{J}},$$

$$\boldsymbol{\nabla}\xi_3 = -(\boldsymbol{\nabla}\xi_1 + \boldsymbol{\nabla}\xi_5), \qquad \boldsymbol{\nabla}\xi_4 = -(\boldsymbol{\nabla}\xi_2 + \boldsymbol{\nabla}\xi_5)$$

are expressed in terms of the *unitary basis vectors* $\boldsymbol{\ell}^1$, $\boldsymbol{\ell}^2$, $\boldsymbol{\ell}^5$ which are the derivatives of the element position vector $\boldsymbol{r}$ with respect to the *independent* coordinates ξ_1, ξ_2 and ξ_5. The element edges are formed by intersection of pairs of zero-coordinates surfaces, and the *edge vectors*

$$\boldsymbol{\ell}_{ab} = \mathcal{J}\,\boldsymbol{\nabla}\xi_a \times \boldsymbol{\nabla}\xi_b$$

are directed along the cross product of the associated coordinate gradients. The edges are given a two-index label deriving from the two coordinate indices appearing in this cross product. The *unitary basis vectors* determine the following eight *edge vectors*

$$\boldsymbol{\ell}_{25} = -\boldsymbol{\ell}_{45} = \boldsymbol{\ell}^1 \qquad \boldsymbol{\ell}_{23} = \boldsymbol{\ell}^5 - \boldsymbol{\ell}^1$$

$$\boldsymbol{\ell}_{35} = -\boldsymbol{\ell}_{15} = \boldsymbol{\ell}^2 \qquad \boldsymbol{\ell}_{34} = \boldsymbol{\ell}^5 - \boldsymbol{\ell}^1 - \boldsymbol{\ell}^2$$

$$\boldsymbol{\ell}_{12} = \boldsymbol{\ell}^5 \qquad\qquad \boldsymbol{\ell}_{41} = \boldsymbol{\ell}^5 - \boldsymbol{\ell}^2$$

with $\boldsymbol{\ell}_{12}$, $\boldsymbol{\ell}_{23}$, $\boldsymbol{\ell}_{34}$, $\boldsymbol{\ell}_{41}$ oriented towards the tip of the pyramid and $\boldsymbol{\ell}_{15}$, $\boldsymbol{\ell}_{25}$, $\boldsymbol{\ell}_{35}$, $\boldsymbol{\ell}_{45}$ arranged counterclockwise when viewed from the tip of the pyramid. The *mixed edges* 15, 25, 35, 45 are in common with a triangular face and the quadrilateral face; the *triangle edges* 12, 23, 34, 41 are shared only by triangular faces.

By counting modulo 4 all the subscripts obtained by varying γ from 1 to 4 and by setting

$$\delta = \gamma + 1$$

the eight basis functions and their curl take the form

$$\boldsymbol{\Omega}_{\gamma\delta}(\boldsymbol{r}) = \eta_{\gamma+2}\,\eta_{\delta+2}\,\boldsymbol{\nabla}\xi_5 - \xi_5(1-\xi_5)\boldsymbol{\nabla}[\eta_{\gamma+2}\,\eta_{\delta+2}]$$

$$\boldsymbol{\Omega}_{\gamma5}(\boldsymbol{r}) = (1-\xi_5)^2 \eta_{\gamma+2}\boldsymbol{\nabla}\eta_{\delta+2}$$

$$\boldsymbol{\nabla} \times \boldsymbol{\Omega}_{\gamma\delta}(\boldsymbol{r}) = -2\,\frac{(\eta_{\gamma+2}\,\boldsymbol{\ell}_{\delta5} + \eta_{\delta+2}\,\boldsymbol{\ell}_{\gamma5})}{\mathcal{J}}$$

$$\boldsymbol{\nabla} \times \boldsymbol{\Omega}_{\gamma5}(\boldsymbol{r}) = \frac{\boldsymbol{\nabla} \times \boldsymbol{\Omega}_{\gamma\delta}(\boldsymbol{r})}{2} + \frac{\boldsymbol{\ell}_{\gamma+2,\delta+2}}{\mathcal{J}}$$

with

$$\eta_\gamma = \frac{\xi_\gamma}{1-\xi_5}, \qquad (1-\xi_5)\boldsymbol{\nabla}\eta_\gamma = \boldsymbol{\nabla}\xi_\gamma + \eta_\gamma\boldsymbol{\nabla}\xi_5$$

For example one gets

$$\boldsymbol{\Omega}_{34}(\boldsymbol{r}) = \eta_1\,\eta_2\,(1-2\xi_5)\,\boldsymbol{\nabla}\xi_5 - \xi_5\,[\eta_2\,\boldsymbol{\nabla}\xi_1 + \eta_1\,\boldsymbol{\nabla}\xi_2]$$

$$\boldsymbol{\nabla} \times \boldsymbol{\Omega}_{34}(\boldsymbol{r}) = 2\,(\eta_1\boldsymbol{\ell}^1 - \eta_2\boldsymbol{\ell}^2)/\mathcal{J}$$

Dependencies among higher order functions arise from linear combinations of the bases which contain one of the following identities as a factor (with $\boldsymbol{\Omega}_{ab} = -\boldsymbol{\Omega}_{ba}$)

$$(1-\xi_5)\,[\eta_\gamma\boldsymbol{\Omega}_{\gamma5} + \eta_{\gamma+2}\boldsymbol{\Omega}_{\gamma+2,5}] = \mathbf{0}, \quad \text{for } \gamma = 1, 2$$

$$(1-\xi_5)\,[\eta_1\boldsymbol{\Omega}_{\gamma1} + \eta_3\boldsymbol{\Omega}_{\gamma3}] + \xi_5\boldsymbol{\Omega}_{\gamma5} = \mathbf{0}, \quad \text{for } \gamma = 2, 4$$

$$(1-\xi_5)\,[\eta_2\boldsymbol{\Omega}_{\gamma2} + \eta_4\boldsymbol{\Omega}_{\gamma4}] + \xi_5\boldsymbol{\Omega}_{\gamma5} = \mathbf{0}, \quad \text{for } \gamma = 1, 3$$

The completeness relations are: $\quad \boldsymbol{\Omega}_{25}(\boldsymbol{r}) - \boldsymbol{\Omega}_{45}(\boldsymbol{r}) = (1-\xi_5)^2\,\boldsymbol{\nabla}\eta_1, \qquad \boldsymbol{\Omega}_{35}(\boldsymbol{r}) - \boldsymbol{\Omega}_{15}(\boldsymbol{r}) = (1-\xi_5)^2\,\boldsymbol{\nabla}\eta_2$

$$\boldsymbol{\Omega}_{25}(\boldsymbol{r}) - \boldsymbol{\Omega}_{45}(\boldsymbol{r}) - \boldsymbol{\Omega}_{23}(\boldsymbol{r}) - \boldsymbol{\Omega}_{34}(\boldsymbol{r}) = \boldsymbol{\nabla}\xi_1 \qquad\qquad \boldsymbol{\nabla} \times [\boldsymbol{\Omega}_{34}(\boldsymbol{r}) + \boldsymbol{\Omega}_{41}(\boldsymbol{r})] = 2\,\boldsymbol{\ell}^1/\mathcal{J}$$

$$\boldsymbol{\Omega}_{35}(\boldsymbol{r}) - \boldsymbol{\Omega}_{15}(\boldsymbol{r}) - \boldsymbol{\Omega}_{34}(\boldsymbol{r}) - \boldsymbol{\Omega}_{41}(\boldsymbol{r}) = \boldsymbol{\nabla}\xi_2 \qquad\qquad \boldsymbol{\nabla} \times [\boldsymbol{\Omega}_{12}(\boldsymbol{r}) + \boldsymbol{\Omega}_{41}(\boldsymbol{r})] = 2\,\boldsymbol{\ell}^2/\mathcal{J}$$

$$\boldsymbol{\Omega}_{12}(\boldsymbol{r}) + \boldsymbol{\Omega}_{23}(\boldsymbol{r}) + \boldsymbol{\Omega}_{34}(\boldsymbol{r}) + \boldsymbol{\Omega}_{41}(\boldsymbol{r}) = \boldsymbol{\nabla}\xi_5 \qquad\qquad \boldsymbol{\nabla} \times [\boldsymbol{\Omega}_{35}(\boldsymbol{r}) + \boldsymbol{\Omega}_{45}(\boldsymbol{r})] = 2\,\boldsymbol{\ell}^5/\mathcal{J}$$

element edge which matches with that of the curl-conforming *zeroth-order* functions of the adjacent element having brick, tetrahedral, or prismatic shapes [11].

Once again, (12) is the sum of two polynomial functions.

1) The curl-free component is a polynomial, because it is the divergence of a polynomial that contains the factor $(1 - \xi_5)$.

2) The nonzero curl component, clearly polynomial, has also polynomial curl, since it contains the factor $(1-\xi_5)$.

It is fascinating how our fractional functions of space $\boldsymbol{\xi}$ unfold into polynomials simply by mapping the pyramid to a cubic cell whose vertices are the intersection points of three edges. As mentioned in Section II, it is reasonable to insist that this also applies to all other higher order functions, if only for uniformity and for energy considerations based on (11). We therefore state the following.

> *POSTULATE:* In terms of the scaled variables, the curl-conforming basis functions of the pyramid are polynomials with polynomial curl.

As postulated, the higher order functions are obtained simply by multiplying the lowest order functions of Table I by polynomials of the space $(\boldsymbol{\eta}, \xi_5)$, and the order of a function

is that of its multiplicative polynomial. The lowest order functions of Table I have zero order (in fact, on the boundary, they match the zero-order functions of adjacent elements).

Expressions (7)–(13) wipe old habits [11] and allow to derive the pyramid's basis functions by shifting to a new paradigm.

1) The vector components of the basis functions and of the curl of the basis functions are polynomials of the variables $\boldsymbol{\eta}$, ξ_5. Unisolvency and base completeness must be proved in the space described by the grandparent variables.

2) Each higher order vector function is obtained by multiplying one vector function of zero order by a scalar generating polynomial which, in turn, is the product of normalized orthogonal polynomials (the same was done in [3]–[6]).

3) The multiplicative polynomials are defined in the grand-parent cubic cell of Fig. 1 (whose vertices are the points of intersection of only three edges and faces).

4) On the pyramid border, the multiplicative polynomials that generate the edge- and face-based functions coincide with those for the adjacent elements, no matter what shape they have.

According to this new paradigm, once the importance of the $(1 - \xi_5)$ factor previously discussed is understood, we immediately derive the volume-based bubble functions and obtain all the others by simply imposing, on cell's boundary, the tangential continuity of the pyramid basis functions with the other known expressions valid for differently shaped cells. So keep in mind that it is only for the sake of brevity that conformity with differently shaped elements is "demonstrated" in Section V "after" the axiomatic definition of the basis functions.

Also note that the dependency relations [see (6) and (9)] ensure that the *homogeneous* polynomials of order p of the $\boldsymbol{\xi}$-domain

$$\xi_j^r \, \xi_{j+1}^s \, \xi_5^t, \quad r + s + t = p \tag{14}$$

are polynomials of order p in ξ_5 of the $(\boldsymbol{\eta}, \xi_5)$-domain

$$\eta_j^r \, \eta_{j+1}^s \left[(1 - \xi_5)^{r+s} \, \xi_5^t \right], \quad r + s + t = p \tag{15}$$

while, the other way around, the product of $(1 - \xi_5)^p$ times a polynomial of order p in η_j is a polynomial of global order p in ξ_j, ξ_{j+2}. In particular, we get

$$(1 - \xi_5)^p \sum_{k=0}^{p} a_k \left(2\eta_j - 1 \right)^k$$

$$= \sum_{k=0}^{p} a_k (1 - \xi_5)^p \left(\eta_j - \eta_{j+2} \right)^k$$

$$= \sum_{k=0}^{p} a_k \left(\xi_j + \xi_{j+2} \right)^{p-k} \left(\xi_j - \xi_{j+2} \right)^k = \sum_{m=0}^{p} b_m \, \xi_j^m \, \xi_{j+2}^{p-m} \tag{16}$$

where the coefficients b_m depend on the coefficients a_k, as well as on the value of p. Equation (16) is useful to assess the global order of the multiplicative polynomials we introduce in Section V. Notice that (14) neglects the condition that ξ_j and ξ_{j+1} are zero at the tip of the pyramid, while (15) takes automatically into account the fact that (14) must vanish at $\xi_5 = 1$. The same is true for (16) which vanishes at $\xi_5 = 1$ for $p \geq 1$, a condition that we would have to impose if we used the expression on the right-hand side of (16).

V. HIGH-ORDER BASIS FUNCTIONS

The edge- and face-based functions are derived by considering two groups: one consisting of functions associated with the *mixed* edges and another associated with the *triangle* edges. Each function is the product of a zero-order vector function times a multiplicative scalar polynomial that we construct by using the *normalized* polynomials $Q_n(x, y)$ of Table II and the *normalized* Jacobi's polynomials of Table III that we readily evaluate for any order using their appropriate recurrence relations [6], [20], [21]. We already used these polynomials to construct the hierarchical bases reported in [3] and [5]; for example, the edge-based polynomials shown in the upper part of [3, Table II] coincide with $Q_n(\xi_a, \xi_b)$ by setting $\chi_{cd} = \xi_5 = (1 - \xi_a - \xi_b)$. Referring back to (16), note

TABLE II
POLYNOMIAL $Q_n(x, y)$

Definition:

$$Q_n(x, y) = \sqrt{2n + 1} \, (x + y)^n \, P_n \left(\frac{x - y}{x + y} \right)$$

where P_n is the Legendre polynomial of order n.

Properties:

$$Q_n(x, y) = (-1)^n \, Q_n(y, x)$$
$$Q_n(x, 0) = \sqrt{2n + 1} \, x^n$$
$$Q_n(0, 0) = 0 \text{ for } n \geq 1$$

Recurrence relation:

$$Q_0(x, y) = 1 \qquad Q_1(x, y) = \sqrt{3} \, (x - y)$$

$$Q_n(x, y) = \frac{1}{n} \left[\sqrt{4n^2 - 1}(x - y) Q_{n-1}(x, y) \right.$$
$$\left. - (n - 1) \sqrt{\frac{2n + 1}{2n - 3}} (x + y)^2 Q_{n-2}(x, y) \right]$$

that (6) and (9) yield

$$Q_n \left(\xi_{\gamma+1}, \xi_{\gamma-1} \right) = (1 - \xi_5)^n \, Q_n \left(\eta_{\gamma+1}, \eta_{\gamma-1} \right)$$
$$= \sqrt{2n + 1} \, (1 - \xi_5)^n \, P_n \left(\eta_{\gamma+1} - \eta_{\gamma-1} \right)$$
$$= (1 - \xi_5)^n \, A_n \left(\eta_{\gamma+1} \right) \tag{17}$$

and that the polynomials of Table III are functions of $(2z - 1)$, with

$$2\eta_{\gamma+1} - 1 = \eta_{\gamma+1} - \eta_{\gamma-1}$$
$$2\eta_\gamma - 1 = \eta_\gamma - \eta_{\gamma+2}. \tag{18}$$

Equation (7) and the first of (18) show that, apart from the normalization constant, the polynomials (17) coincide with the shifted scaled Legendre polynomials

$$P_n \left[2 \left(\frac{\xi_{\gamma+1}}{1 - \xi_5} \right) - 1 \right] (1 - \xi_5)^n = \frac{Q_n \left(\xi_{\gamma+1}, \xi_{\gamma-1} \right)}{\sqrt{2n + 1}} \tag{19}$$

used also in [17] and [22].

On the pyramid border, the edge- and face-based functions match those given in [6] for the tetrahedron, the brick, and the prism, and this guarantees the mutual orthogonality of the edge-based functions on the edges and faces of the pyramid, as well as the mutual orthogonality of the face-based functions on the pyramid's faces. The edge- and face-based functions are not mutually orthogonal for integrals on the volume of the pyramid. They can be rendered mutually orthogonal on the volume by adding to each of these functions an appropriate linear combination of the volume-based functions.

A. Volume-Based Functions

Volume-based vector functions have zero tangential component on all cell faces and are obtained by inspection observing that the gradients $\nabla \eta_j = -\nabla \eta_{j+2}$ are orthogonal to both faces $\eta_j = 0$ and $\eta_{j+2} = 0$. The three fundamental bubble functions

TABLE III
NORMALIZED ORTHOGONAL POLYNOMIALS

Normalized polynomial $\mathcal{P}_n(z)$	Normalization coefficient	Weight function
$A_n(z) = N_a\, P_n^{(0,0)}(2z-1)$	$N_a = \sqrt{2n+1}$	1
$B_n(z) = N_b\, P_n^{(2,2)}(2z-1)$	$N_b = \sqrt{\dfrac{(2n+5)(n+3)(n+4)}{3(n+1)(n+2)}}$	$3(1-z)^2\, z^2$
$C_n^{(m)}(z) = N_c\, P_n^{(2m+1,2)}(2z-1)$	$N_c = \sqrt{\dfrac{(2m+n+2)(2m+n+3)(2m+2n+4)}{(n+1)(n+2)}}$	$(1-z)^{2m+1}\, z^2$
$D_n(z) = N_d\, P_n^{(2,0)}(2z-1)$	$N_d = \sqrt{2n+3}$	$(1-z)^2$

The polynomials $\mathcal{P}_n(z)$ in the left column are obtained by rescaling the shifted Jacobi polynomials $P_n^{(\alpha\beta)}(2z-1)$ of order n, being $P_n = P_n^{(00)}$ the Legendre polynomial. The system of polynomials $P_n^{(\alpha\beta)}(2z-1)$ is orthogonal on the interval $[0,1]$ with respect to the weight function $(1-z)^\alpha\, z^\beta$. The normalization coefficients depend on the order n of the polynomial itself, as well as on the value of the integer m that defines the exponent α of the corresponding weight function, reported in the right column for clarity. The polynomial systems listed in the left column satisfy the orthogonality relation

$$\int_0^1 w(z)\,\mathcal{P}_n(z)\,\mathcal{P}_\ell(z)\,\mathrm{d}z = \delta_{n\ell}$$

being $\delta_{n\ell}$ the Kronecker delta function. These polynomials have a zero derivative for $n=0$, while for $n>0$ we have

$$\frac{\mathrm{d}}{\mathrm{d}z}A_n(z) = (n+1)\,N_a\,\frac{P_{n+1}(2z-1)-(2z-1)P_n(2z-1)}{2z(z-1)} \qquad \frac{\mathrm{d}}{\mathrm{d}z}B_n(z) = (n+5)\,N_b\,P_{n-1}^{(3,3)}(2z-1)$$

$$\frac{\mathrm{d}}{\mathrm{d}z}C_n^{(m)}(z) = (2m+n+4)\,N_c\,P_{n-1}^{(2m+2,3)}(2z-1) \qquad \frac{\mathrm{d}}{\mathrm{d}z}D_n(z) = (n+3)\,N_f\,P_{n-1}^{(3,1)}(2z-1)$$

of the lowest order possible

$$\begin{cases} \boldsymbol{\Omega}_{B1} = \xi_5(1-\xi_5)\eta_1\eta_3\nabla\eta_4 \\ \qquad = -\xi_5\eta_1\eta_3(\nabla\xi_2 + \eta_2\nabla\xi_5) \\ \boldsymbol{\Omega}_{B2} = \xi_5(1-\xi_5)\eta_2\eta_4\nabla\eta_1 \\ \qquad = \xi_5\eta_2\eta_4(\nabla\xi_1 + \eta_1\nabla\xi_5) \\ \boldsymbol{\Omega}_{B3} = \eta_1\eta_2\eta_3\eta_4\nabla\xi_5 \end{cases} \qquad (20)$$

have a nonphysical singular curl in $\xi_5 = 1$ and therefore do not belong to the polynomial base. In fact, the lowest order polynomial functions with polynomial curl are obtained simply by multiplying (20) by $(1-\xi_5)$, which immediately allows us to write all the higher order polynomial bubble functions in the form

$$\begin{cases} \boldsymbol{\Omega}_{ijk}^{B1} = (1-\xi_5)\,B_{j-1}(\eta_1)\,B_{i-1}(\xi_5)\,A_k(\eta_2)\,\boldsymbol{\Omega}_{B1} \\ \boldsymbol{\Omega}_{ijk}^{B2} = (1-\xi_5)\,B_{j-1}(\eta_2)\,B_{i-1}(\xi_5)\,A_k(\eta_1)\,\boldsymbol{\Omega}_{B2} \\ \boldsymbol{\Omega}_{ijk}^{B3} = (1-\xi_5)\,B_{i-1}(\eta_1)B_{j-1}(\eta_2)\,D_k(\xi_5)\,\boldsymbol{\Omega}_{B3}. \end{cases} \qquad (21)$$

In terms of the zeroth-order vector functions of Table I, the bubbles (21) read as follows:

$$\begin{cases} \boldsymbol{\Omega}_{ijk}^{15} = \boldsymbol{\Omega}_{ijk}^{B1} = \xi_5\eta_1\,B_{j-1}(\eta_1)\,B_{i-1}(\xi_5)\,A_k(\eta_2)\,\boldsymbol{\Omega}_{15} \\ \boldsymbol{\Omega}_{ijk}^{25} = \boldsymbol{\Omega}_{ijk}^{B2} = \xi_5\eta_2\,B_{j-1}(\eta_2)\,B_{i-1}(\xi_5)\,A_k(\eta_1)\,\boldsymbol{\Omega}_{25} \\ \boldsymbol{\Omega}_{ijk}^{B3} = (1-\xi_5)\,\eta_1\eta_2\eta_3\eta_4 \\ \qquad\quad \times\big[B_{i-1}(\eta_1)B_{j-1}(\eta_2)\,D_k(\xi_5)\big]\,\nabla\xi_5 \end{cases} \qquad (22)$$

being $\nabla\xi_5$ the sum of the functions $\boldsymbol{\Omega}_{12}$, $\boldsymbol{\Omega}_{23}$, $\boldsymbol{\Omega}_{34}$, and $\boldsymbol{\Omega}_{41}$ associated with the triangle edges (see Table I at bottom left).

Before proceeding further, let us see the differences with respect to the bubble functions proposed by other authors, bearing in mind that our bubbles (21) contain the factor $(1-\xi_5)^n$ with $n=1$, which is the minimum value of n that guarantees polynomial curls. A factor $(1-\xi_5)^n$ appears in the expression of the bubble functions of the fourth family of [17, eqs. (9.26), (B.35)] and in all those of [16], but in those expressions, n depends on the maximum value between two of the indices i, j, and k and can be greater than unity. Since the other basis functions have no factors that depend on the values of a pair of indexes, it is not clear to us why some bubbles should contain a factor $(1-\xi_5)^n$ instead of the factor $(1-\xi_5)$ as in the case of our bubbles (21). By substituting the functions of the fourth family of [17] for our $\boldsymbol{\Omega}_{ijk}^{B3}$, assuming that they are *equivalent*, we have found the occurrence of spurious modes. We also observe that the expression of the higher order functions in [17] involve integrated Legendre polynomials, while we always use orthogonal Jacobi's polynomials. It is certainly possible to use integrated Legendre polynomials instead of orthogonal Jacobi's polynomials (normalized as in Table III); we have tried it, and we have seen that, by doing so, the mass matrix CN increases by at least two orders of magnitude.

Our p-order complete curl-conforming set has a total of $3p^2(p+1)$ bubble functions, since each $\boldsymbol{\Omega}_{B1}$, $\boldsymbol{\Omega}_{B2}$, and $\boldsymbol{\Omega}_{B3}$ generates $p^2(p+1)$ functions hierarchically organized as follows.

1) For $p=0$, there are no bubble functions.
2) For $p=1$, the set is made up of $\boldsymbol{\Omega}_{110}^B$, $\boldsymbol{\Omega}_{111}^B$.

TABLE IV
BUBBLE FUNCTIONS' CURLS

$$\boldsymbol{\nabla} \times \boldsymbol{\Omega}_{ijk}^{B1} = \frac{A_k(\eta_2)}{\mathcal{J}} \Big[\eta_1\, \eta_3\, B_{j-1}(\eta_1)\, U_i(\xi_5)\, \boldsymbol{\ell}^1 \\ - \xi_5\, B_{i-1}(\xi_5)\, V_j(\eta_1)\, \boldsymbol{\ell}^T \Big]$$

$$\boldsymbol{\nabla} \times \boldsymbol{\Omega}_{ijk}^{B2} = \frac{A_k(\eta_1)}{\mathcal{J}} \Big[\eta_2\, \eta_4\, B_{j-1}(\eta_2)\, U_i(\xi_5)\, \boldsymbol{\ell}^2 \\ - \xi_5\, B_{i-1}(\xi_5)\, V_j(\eta_2)\, \boldsymbol{\ell}^T \Big]$$

$$\boldsymbol{\nabla} \times \boldsymbol{\Omega}_{ijk}^{B3} = \frac{D_k(\xi_5)}{\mathcal{J}} \Big[\eta_1 \eta_3\, B_{i-1}(\eta_1)\, V_j(\eta_2)\, \boldsymbol{\ell}^1 \\ - \eta_2 \eta_4\, B_{j-1}(\eta_2)\, V_i(\eta_1)\, \boldsymbol{\ell}^2 \Big]$$

$$\boldsymbol{\ell}^T = \boldsymbol{\ell}^5 - \eta_1\, \boldsymbol{\ell}^1 - \eta_2\, \boldsymbol{\ell}^2$$

$$\begin{cases} T_n(z) = z(1-z)\, \dfrac{\mathrm{d}}{\mathrm{d}z} B_{n-1}(z) \\ U_n(z) = T_n(z) - (3z-1)\, B_{n-1}(z) \\ V_n(z) = T_n(z) - (2z-1)\, B_{n-1}(z) \quad n = i \text{ or } j \end{cases}$$

3) For $p \geq 2$, one has to increment the set of order $(p-1)$ with $p(3p-1)$ polynomials $\boldsymbol{\Omega}_{ijk}^B$ obtained for

$$i = p, \quad j = 1 \text{ to } p, \ k = 0 \text{ to } p-1$$
$$i = 1 \text{ to } p-1, \quad j = p, \ k = 0 \text{ to } p-1$$
$$i = 1 \text{ to } p, \quad j = 1 \text{ to } p, \ k = p$$

where $\boldsymbol{\Omega}_{ijk}^B$ stands for $\boldsymbol{\Omega}_{ijk}^{B1}$, $\boldsymbol{\Omega}_{ijk}^{B2}$, or $\boldsymbol{\Omega}_{ijk}^{B3}$.

Table IV reports the curls of the bubble functions in terms of the *unitary basis vectors* of Table I.

For the maximum value p assumed by the indexes i, j, and k, the component in $\boldsymbol{\nabla}\xi_5$ of the bubbles (21) is of order $(p+1)$ in η_1, η_2, and ξ_5. The $\boldsymbol{\nabla}\xi_1$ component of the bubbles (21) is of order p in η_1 and $(p+1)$ in η_2; similarly, the $\boldsymbol{\nabla}\xi_2$ component is of order p in η_2 and $(p+1)$ in η_1. The same happens for the vector functions associated with the triangle and mixed edges that we consider in the following two subsections. All these do not happen by accident, and it is used to demonstrate the completeness of the bases in the Appendix.

B. Functions Associated With the Mixed Edges

Higher order vector functions

$$\boldsymbol{\Omega}_{ijk}^{\gamma 5} = H_{ijk}^{\gamma 5}\, \boldsymbol{\Omega}_{\gamma 5} \tag{23}$$

associated with the mixed edge $\gamma 5$ (for $\gamma = 1, 2, 3, 4$) are obtained simply by multiplying the zeroth-order function

$$\boldsymbol{\Omega}_{\gamma 5} = (\eta_\gamma - 1)(1 - \xi_5)\left[\eta_{\gamma+1}\boldsymbol{\nabla}\xi_5 + \boldsymbol{\nabla}\xi_{\gamma+1}\right] \tag{24}$$

by $(p+1)(3p+2)/2$ hierarchical polynomials

$$\begin{bmatrix} H_{00k}^{\gamma 5} \\ H_{0jk}^{\gamma 5} \\ H_{i0k}^{\gamma 5} \end{bmatrix} = \begin{bmatrix} (1-\xi_5)^k \\ \eta_\gamma\, B_{j-1}(\eta_\gamma) \\ \xi_5\,(1-\xi_5)^k\, C_{i-1}^{(k)}(\xi_5) \end{bmatrix} A_k(\eta_{\gamma+1}) \tag{25}$$

obtained for $k + i \leq p$. Set (25) has $(p+1)$ edge-based polynomials $H_{00k}^{\gamma 5}$ that naturally form a hierarchical subset for k ranging from 0 to p, in the sense that for $p = 0$, the subset

contains only the polynomial $H_{000}^{\gamma 5}$, while for $p \geq 1$, one has to increment the set of order $(p-1)$ with the polynomial $H_{00p}^{\gamma 5}$.

We then have $p(p+1)$ *face-based* polynomials $H_{0jk}^{\gamma 5}$ that vanish on face γ (where $\eta_\gamma = 0$) and are based on the $\xi_5 = 0$ face; they are hierarchically organized as follows.

1) For $p = 1$, the set consists of the polynomials $H_{010}^{\gamma 5}$ and $H_{011}^{\gamma 5}$.
2) For $p > 1$, the set of order $(p - 1)$ is augmented by adding p polynomials $H_{0pk}^{\gamma 5}$, obtained for $k = 0, 1, \ldots, p - 1$, plus p polynomials $H_{0jp}^{\gamma 5}$ obtained for $j = 1, \ldots, p$.

Finally, we have $p(p + 1)/2$ *face-based* polynomials $H_{i0k}^{\gamma 5}$ that vanish for $\xi_5 = 0$ and are different from zero on the $\xi_\gamma = 0$ triangular face; that is, they are based on face γ and hierarchically organized as follows.

1) For $p = 1$, the set consists of the polynomial $H_{100}^{\gamma 5}$.
2) For $p > 1$, one has to increment the set of order $(p - 1)$ with p polynomials $H_{i0k}^{\gamma 5}$ obtained for $k = 0, 1, \ldots, p - 1$ with $i = p - k$.

(Note that the number of polynomials indicated here holds for any mixed edge and does not depend on the shape of the cell, be it a pyramid or a triangular prism [5], [6].)

To show that the edge-based functions $H_{00k}^{\gamma 5}\,\boldsymbol{\Omega}_{\gamma 5}$ conform to the basis function of adjacent cells, we observe that on the quadrilateral face $\xi_5 = 0$, the simplified expression

$$H_{00k}^{\gamma 5}\Big|_{\xi_5=0} = A_k(\xi_{\gamma+1}) = \sqrt{2k+1}\, P_k(\xi_{\gamma+1} - \xi_{\gamma-1}) \tag{26}$$

matches that of the edge-based polynomials given in [5] for the prism, and in [4] for the brick while, to prove conformity on the triangular face $\eta_\gamma = 0$, recall that

$$H_{00k}^{\gamma 5}\Big|_{\eta_\gamma=0} = (1 - \xi_5)^k\, A_k(\eta_{\gamma+1}) = Q_k(\xi_{\gamma+1}, \xi_{\gamma-1}) \tag{27}$$

and then observe that for $(\xi_{\gamma+1}, \xi_{\gamma-1}) = (\xi_a, \xi_b)$, the polynomials (27) coincide with the edge-based polynomials reported in the upper part of [3, Table II] obtained for $\chi_{cd} = \xi_5 = (1 - \xi_a - \xi_b)$. Equally simply, it is proved that on the triangular face, the multiplicative polynomials $H_{00k}^{\gamma 5}$ coincide with those of the triangular prism given in [5, Table III].

As for the face-based polynomials $H_{0jk}^{\gamma 5}$, we note that on the quadrilateral face $\xi_5 = 0$, we have $\eta_\gamma = \xi_\gamma$, so that we get

$$H_{0jk}^{\gamma 5}\Big|_{\xi_5=0} = \xi_\gamma\, N_a\, N_b\, P_k(\xi_{\gamma+1} - \xi_{\gamma-1})\, P_{j-1}^{(22)}(\xi_\gamma - \xi_{\gamma+2}) \tag{28}$$

which is the same expression holding for the face-based polynomials of the brick cell reported in [4, eq. (12)]. (The N_a and N_b values are obtained from Table II.)

Finally, and in a similar way, to demonstrate the conformity of the polynomials $H_{i0k}^{\gamma 5}$ based on the triangular face $\xi_\gamma = 0$ with those of the adjacent cell (possibly of tetrahedral or prismatic shape), it is sufficient to compare their expression with those reported in [5, Table III] and [3, Table II].

As already done in [3]–[5], the sign of the vector functions (23) must be adjusted if the orientation of the mixed edge is opposite to the "reference" one, or different from that of the adjacent cells, as a consequence of (27) and of the

TABLE V
CURLS OF THE VECTOR FUNCTIONS ASSOCIATED WITH THE MIXED EDGES

$$\nabla \times \mathbf{\Omega}_{00k}^{15} = \frac{(1-\xi_5)^k A_k(\eta_2)}{\mathcal{J}} \left[\boldsymbol{\ell}^T - (2+k)\eta_3 \boldsymbol{\ell}^1 \right]$$

$$\nabla \times \mathbf{\Omega}_{i0k}^{15} = \frac{(1-\xi_5)^k A_k(\eta_2)}{\mathcal{J}} \left[\xi_5\, C_{i-1}^{(k)}(\xi_5)\, \boldsymbol{\ell}^T - \eta_3 V_{ik}(\xi_5)\, \boldsymbol{\ell}^1 \right]$$

$$\nabla \times \mathbf{\Omega}_{00k}^{25} = \frac{(1-\xi_5)^k A_k(\eta_3)}{\mathcal{J}} \left[\boldsymbol{\ell}^T - (2+k)\eta_4 \boldsymbol{\ell}^2 \right]$$

$$\nabla \times \mathbf{\Omega}_{i0k}^{25} = \frac{(1-\xi_5)^k A_k(\eta_3)}{\mathcal{J}} \left[\xi_5\, C_{i-1}^{(k)}(\xi_5)\, \boldsymbol{\ell}^T - \eta_4 V_{ik}(\xi_5)\, \boldsymbol{\ell}^2 \right]$$

$$\nabla \times \mathbf{\Omega}_{00k}^{35} = \frac{(1-\xi_5)^k A_k(\eta_4)}{\mathcal{J}} \left[\boldsymbol{\ell}^T + (2+k)\eta_1 \boldsymbol{\ell}^1 \right]$$

$$\nabla \times \mathbf{\Omega}_{i0k}^{35} = \frac{(1-\xi_5)^k A_k(\eta_4)}{\mathcal{J}} \left[\xi_5\, C_{i-1}^{(k)}(\xi_5)\, \boldsymbol{\ell}^T + \eta_1 V_{ik}(\xi_5)\, \boldsymbol{\ell}^1 \right]$$

$$\nabla \times \mathbf{\Omega}_{00k}^{45} = \frac{(1-\xi_5)^k A_k(\eta_1)}{\mathcal{J}} \left[\boldsymbol{\ell}^T + (2+k)\eta_2 \boldsymbol{\ell}^2 \right]$$

$$\nabla \times \mathbf{\Omega}_{i0k}^{45} = \frac{(1-\xi_5)^k A_k(\eta_1)}{\mathcal{J}} \left[\xi_5\, C_{i-1}^{(k)}(\xi_5)\, \boldsymbol{\ell}^T + \eta_2 V_{ik}(\xi_5)\, \boldsymbol{\ell}^2 \right]$$

$$\boldsymbol{\ell}^T = \boldsymbol{\ell}^5 - \eta_1\, \boldsymbol{\ell}^1 - \eta_2\, \boldsymbol{\ell}^2$$

$$V_{ik}(z) = [(3+k)z - 1]\, C_{i-1}^{(k)}(z) - z(1-z)\frac{\mathrm{d}}{\mathrm{d}z} C_{i-1}^{(k)}(z)$$

$$\nabla \times \mathbf{\Omega}_{0jk}^{15} = \frac{A_k(\eta_2)}{\mathcal{J}} \left\{ [T_j(\eta_1) - B_{j-1}(\eta_1)]\, \eta_1\, \boldsymbol{\ell}^1 + V_j(\eta_1)\left(\eta_2\, \boldsymbol{\ell}^2 - \boldsymbol{\ell}^5\right) \right\}$$

$$\nabla \times \mathbf{\Omega}_{0jk}^{25} = \frac{A_k(\eta_3)}{\mathcal{J}} \left\{ [T_j(\eta_2) - B_{j-1}(\eta_2)]\, \eta_2\, \boldsymbol{\ell}^2 + V_j(\eta_2)\left(\eta_1\, \boldsymbol{\ell}^1 - \boldsymbol{\ell}^5\right) \right\}$$

$$\nabla \times \mathbf{\Omega}_{0jk}^{35} = \frac{A_k(\eta_4)}{\mathcal{J}} \left\{ [T_j(\eta_3) + B_{j-1}(\eta_3)]\, \eta_1\, \boldsymbol{\ell}^1 + V_j(\eta_3)\left(\eta_2\, \boldsymbol{\ell}^2 - \boldsymbol{\ell}^5\right) \right\} \qquad T_j(z) = z(1-z)\frac{\mathrm{d}}{\mathrm{d}z} B_{j-1}(z)$$

$$\nabla \times \mathbf{\Omega}_{0jk}^{45} = \frac{A_k(\eta_1)}{\mathcal{J}} \left\{ [T_j(\eta_4) + B_{j-1}(\eta_4)]\, \eta_2\, \boldsymbol{\ell}^2 + V_j(\eta_4)\left(\eta_1\, \boldsymbol{\ell}^1 - \boldsymbol{\ell}^5\right) \right\} \qquad V_j(z) = T_j(z) - (2z-1)\, B_{j-1}(z)$$

symmetry relations of the Legendre polynomials

$$P_k\left(\eta_{\gamma+1} - \eta_{\gamma-1}\right) = (-1)^k P_k\left(\eta_{\gamma-1} - \eta_{\gamma+1}\right). \qquad (29)$$

Table V reports the curls of the vector functions (23) in terms of the *unitary basis vectors* of Table I.

C. Functions Associated With the Triangle Edges

To lighten the notation used to define the basis functions associated with the triangle edge $\xi_\gamma = \xi_\delta = 0$ (for $\gamma = 1, 2, 3, 4$, and $\delta = \gamma + 1$), henceforth we set

$$\widetilde{\xi}_{\gamma\delta} = (1-\xi_5)\left(1-\eta_\gamma\right)(1-\eta_\delta) = (1-\xi_5)\,\eta_{\gamma+2}\,\eta_{\delta+2} \qquad (30)$$

highlighting the following key features.

1) On face $\eta_\delta = 0$ and face $\eta_\gamma = 0$, one gets $\widetilde{\xi}_{\gamma\delta} = \xi_{\gamma+2}$ and $\widetilde{\xi}_{\gamma\delta} = \xi_{\delta+2}$, respectively.
2) $\widetilde{\xi}_{\gamma\delta} = (1-\xi_5)$ along the edge $\gamma\delta$ where $\eta_{\gamma+2}\,\eta_{\delta+2} = 1$, while it vanishes on the two triangular faces opposite to the edge at issue where $\eta_{\gamma+2}\,\eta_{\delta+2} = 0$.
3) The gradient of (30) takes the polynomial expression

$$\nabla\widetilde{\xi}_{\gamma\delta} = \left(\eta_\gamma\,\eta_\delta - 1\right)\nabla\xi_5 - \eta_{\delta+2}\nabla\xi_\gamma - \eta_{\gamma+2}\nabla\xi_\delta. \qquad (31)$$

That said, the higher order vector functions

$$\mathbf{\Omega}_{ijk}^{\gamma\delta} = H_{ijk}^{\gamma\delta}\, \mathbf{\Omega}_{\gamma\delta} \qquad (32)$$

are simply obtained by multiplying the lowest order function $\mathbf{\Omega}_{\gamma\delta}$ by $(p+1)^2$ hierarchical polynomials

$$\begin{bmatrix} H_{00k}^{\gamma\delta} \\ H_{0jk}^{\gamma\delta} \\ H_{i0k}^{\gamma\delta} \end{bmatrix} = \begin{bmatrix} Q_k\left(\xi_5, \widetilde{\xi}_{\gamma\delta}\right) \\ \xi_\gamma\, C_{j-1}^{(k)}(\xi_\gamma)\, Q_k\left(\xi_5, \xi_{\gamma+2}\right) \\ \xi_\delta\, C_{i-1}^{(k)}(\xi_\delta)\, Q_k\left(\xi_5, \xi_{\delta+2}\right) \end{bmatrix} \qquad (33)$$

which all have a gradient of polynomial form in the space $(\boldsymbol{\eta}, \xi_5)$. This implies that the curl of (32) takes a polynomial form in the space $(\boldsymbol{\eta}, \xi_5)$, since $H_{ijk}^{\gamma\delta}$, $\mathbf{\Omega}_{\gamma\delta}$ and its curl have the polynomial form in this space. [The polynomial form of $\nabla Q_k(\xi_5, \widetilde{\xi}_{\gamma\delta})$ stems from (31).]

Set (33) has $(p+1)$ *edge-based* polynomials $H_{00k}^{\gamma\delta}$; that is, for $p = 0$, this subset is simply formed by $H_{000}^{\gamma\delta}$, while, for $p \geq 1$, one has to increment the subset of order $(p-1)$ with the polynomial $H_{00p}^{\gamma\delta}$.

Set (33) then has $p(p+1)/2$ polynomials $H_{0jk}^{\gamma\delta}$ based on the $\xi_\delta = \eta_\delta = 0$ triangular face, organized as follows.

1) For $p = 1$, the set consists of the functions $H_{010}^{\gamma\delta}$.
2) For $p > 1$, one has to increment the set of order $(p-1)$ with p functions $H_{0jk}^{\gamma\delta}$ obtained for $k = 0, 1, \ldots, p-1$ with $j = p - k$.

Finally, the $p(p+1)/2$ polynomials $H_{i0k}^{\gamma\delta}$ based on the $\xi_\gamma = \eta_\gamma = 0$ triangular face are hierarchically organized as follows.

1) For $p = 1$, the set consists of the polynomial $H_{100}^{\gamma\delta}$.
2) For $p > 1$, one has to increment the set of order $(p-1)$ with p polynomials $H_{i0k}^{\gamma\delta}$ obtained for $k = 0, 1, \ldots, p-1$ with $i = p - k$.

The curls of the functions (32) are given in Table VI.

The vector functions (32) naturally conform to the basis functions of adjacent cells. For example, along the $\gamma\delta$-edge, one gets $\widetilde{\xi}_{\gamma\delta} = 1 - \xi_5$ and

$$H_{00k}^{\gamma\delta}\Big|_{\xi_\gamma=\xi_\delta=0} = Q_k(\xi_5, 1-\xi_5)$$

$$= \sqrt{2k+1}\, P_k(2\xi_5 - 1) \qquad (34)$$

which proves that $H_{00k}^{\gamma\delta}$ conforms to the edge-based polynomials given in [3], [5], apart from a possible sign adjustment.

TABLE VI

CURLS OF THE VECTOR FUNCTIONS ASSOCIATED WITH THE TRIANGLE EDGES

EDGE-BASED FUNCTIONS' CURL - The curls (in terms of the *unitary basis vectors* of Table I) are

$$\nabla \times \mathbf{\Omega}_{00k}^{12} = (2+k)\, Q_k(\xi_5, \widetilde{\xi}_{12}) \left[-\eta_3 \boldsymbol{\ell}^1 + \eta_4 \boldsymbol{\ell}^2 \right] / \mathcal{J} \qquad \nabla \times \mathbf{\Omega}_{00k}^{34} = (2+k)\, Q_k(\xi_5, \widetilde{\xi}_{34}) \left[+\eta_1 \boldsymbol{\ell}^1 - \eta_2 \boldsymbol{\ell}^2 \right] / \mathcal{J}$$

$$\nabla \times \mathbf{\Omega}_{00k}^{23} = (2+k)\, Q_k(\xi_5, \widetilde{\xi}_{23}) \left[-\eta_1 \boldsymbol{\ell}^1 - \eta_4 \boldsymbol{\ell}^2 \right] / \mathcal{J} \qquad \nabla \times \mathbf{\Omega}_{00k}^{41} = (2+k)\, Q_k(\xi_5, \widetilde{\xi}_{41}) \left[+\eta_3 \boldsymbol{\ell}^1 + \eta_2 \boldsymbol{\ell}^2 \right] / \mathcal{J}$$

FACE-BASED FUNCTIONS' CURL - With reference to (37) or (38) we first compute the gradients

$$\nabla H_{0jk}^{\gamma\delta} = R_{jk}^a[\gamma]\, \nabla\xi_\gamma + R_{jk}^b[\gamma]\, \nabla\xi_5; \qquad \nabla\left(\eta_{\delta+2}\, H_{0jk}^{\gamma\delta} \right) = \eta_{\delta+2}\, \nabla H_{0jk}^{\gamma\delta} + (1-\xi_5)\,(\eta_\delta \nabla\xi_5 - \nabla\xi_\delta)\, H_{0jk}^{\gamma\delta};$$

$$\nabla H_{i0k}^{\gamma\delta} = R_{ik}^a[\delta]\, \nabla\xi_\delta + R_{ik}^b[\delta]\, \nabla\xi_5; \qquad \nabla\left(\eta_{\gamma+2}\, H_{i0k}^{\gamma\delta} \right) = \eta_{\gamma+2}\, \nabla H_{i0k}^{\gamma\delta} + (1-\xi_5)\,(\eta_\gamma \nabla\xi_5 - \nabla\xi_\gamma)\, H_{i0k}^{\gamma\delta}$$

where

$$R_{nk}^a[A] = S_k^a(\xi_5, \xi_{A+2})\, C_{n-1}^{(k)}(\xi_A) + \xi_A\, Q_k(\xi_5, \xi_{A+2})\, \frac{\mathrm{d}}{\mathrm{d}\xi_A} C_{n-1}^{(k)}(\xi_A); \quad R_{nk}^b[A] = \xi_A\,(k+1) S_k^b(\xi_5, \xi_{A+2})\, C_{n-1}^{(k)}(\xi_A)$$

$$\xi_A = (1-\xi_5)\,\eta_A; \quad \xi_{A+2} = (1-\xi_5)(1-\eta_A) = (1-\xi_5)\,\eta_{A+2}$$

$$S_k^a(x,y) = \frac{1}{2y} \left[\left(\frac{2(2k+1)x}{x+y} - (k+1)(x-3y+3) + 2 \right) Q_k(x,y) - (k+1)\frac{1-x-y}{x+y}\sqrt{\frac{2k+1}{2k+3}} Q_{k+1}(x,y) \right]$$

$$S_k^b(x,y) = \frac{1}{2xy} \left[(x-y)Q_k(x,y) - \frac{\sqrt{2k+1}}{\sqrt{2k+3}}Q_{k+1}(x,y) \right]$$

Note that $H_{i0k}^{\gamma\delta}$ and $\nabla H_{i0k}^{\gamma\delta}$ are obtained by exchanging γ with δ in the expressions that hold for $H_{0jk}^{\gamma\delta}$ and $\nabla H_{0jk}^{\gamma\delta}$. The *edge vectors* components of the curl of the functions (37) is then computed by using the following formulas for $\gamma = 1,2,3,4$; $\delta = \gamma+1$ computed modulo 4, and with $\nabla\xi_a \times \nabla\xi_b = \boldsymbol{\ell}_{ab}/\mathcal{J}$

$$\nabla \times \begin{bmatrix} \mathbf{\Omega}_{0jk}^{\gamma\delta} \\ \mathbf{\Omega}_{i0k}^{\gamma\delta} \end{bmatrix} = \nabla \begin{bmatrix} H_{0jk}^{\gamma\delta} \\ H_{i0k}^{\gamma\delta} \end{bmatrix} \times \mathbf{\Omega}_{\gamma\delta} - \frac{2\,(\eta_{\gamma+2}\,\boldsymbol{\ell}_{\delta5} + \eta_{\delta+2}\,\boldsymbol{\ell}_{\gamma5})}{\mathcal{J}} \begin{bmatrix} H_{0jk}^{\gamma\delta} \\ H_{i0k}^{\gamma\delta} \end{bmatrix}$$

$$\mathbf{\Omega}_{\gamma\delta} = \xi_5\,\eta_{\delta+2}\nabla\xi_\gamma + \xi_5\,\eta_{\gamma+2}\nabla\xi_\delta + [\eta_{\gamma+2}\,\eta_{\delta+2}\,(1-2\xi_5) + \xi_5\,(\eta_{\gamma+2} + \eta_{\delta+2})]\,\nabla\xi_5$$

$$\nabla \times \mathbf{\Omega}_{\gamma\delta}(\boldsymbol{r}) = -2\,(\eta_{\gamma+2}\,\boldsymbol{\ell}_{\delta5} + \eta_{\delta+2}\,\boldsymbol{\ell}_{\gamma5})/\mathcal{J}$$

We recommend quadrature formulas with samples inside the element to avoid numerical problems due to the expressions of S_k^a, S_k^b provided above. Formulas to compute S_k^a and S_k^b for x and/or y equal to zero are however given below.

$S_0^a(x,y) = 1;$ $\qquad S_1^a(x,y) = \sqrt{3}\,(1-2y);$ $S_2^a(x,y) = \sqrt{5}\,\left[3\left(y^2 - x^2\right) + 2(2x - y - 3xy) \right]$ For $k \geq 1$ use the following limits: $S_k^a(x,0) = \sqrt{2k+1}\,\left[x + k^2(1-x) \right] x^{k-1}$ $S_k^a(0,y) = \sqrt{2k+1}\,\left[y - k(1-y) \right](-1)^k\, y^{k-1}$ that yield $S_k^a(0,0) = 0$ for $k \geq 2$	$S_0^b(x,y) = 0;$ $\qquad S_1^b(x,y) = \sqrt{3};$ $S_2^b(x,y) = \sqrt{5}\,2\,(x-y)$ For $k \geq 1$ use the following limits: $S_k^b(x,0) = \sqrt{2k+1}\,\left(k\, x^{k-1} \right)$ $S_k^b(0,y) = \sqrt{2k+1}\,(-1)^{k+1}\left(k\, y^{k-1} \right)$ that yield $S_k^b(0,0) = 0$ for $k \geq 2$

Conformity on the triangular faces γ and δ descends from the fact that, on these faces, $H_{00k}^{\gamma\delta}$ takes the same form as (27)

$$H_{00k}^{\gamma\delta}\Big|_{\xi_\gamma=0} = Q_k(\xi_5, \xi_{\delta+2}) \qquad (35)$$

$$H_{00k}^{\gamma\delta}\Big|_{\xi_\delta=0} = Q_k(\xi_5, \xi_{\gamma+2}). \qquad (36)$$

Similarly, the conformity of the face-based functions with those in [3], [5] is demonstrated by comparing their expression with those reported in [5, Table III] and [3, Table II].

In applications, the functions

$$\mathbf{\Omega}_{0jk}^{\gamma\delta} = H_{0jk}^{\gamma\delta}\, \mathbf{\Omega}_{\gamma\delta}; \quad \mathbf{\Omega}_{i0k}^{\gamma\delta} = H_{i0k}^{\gamma\delta}\, \mathbf{\Omega}_{\gamma\delta} \qquad (37)$$

can be replaced by

$$\begin{cases} \widetilde{\mathbf{\Omega}}_{0jk}^{\gamma\delta} &= \eta_{\delta+2}\, H_{0jk}^{\gamma\delta}\, \mathbf{\Omega}_\delta \\ \widetilde{\mathbf{\Omega}}_{i0k}^{\gamma\delta} &= \eta_{\gamma+2}\, H_{i0k}^{\gamma\delta}\, \mathbf{\Omega}_\gamma \end{cases} \qquad (38)$$

where, as indicated by the subscripts used

$$\mathbf{\Omega}_\delta = \xi_{\gamma+2}\, \nabla\xi_5 - \xi_5\nabla\xi_{\gamma+2} = \left(1-\xi_\gamma\right)\nabla\xi_5 + \xi_5\nabla\xi_\gamma$$

$$\mathbf{\Omega}_\gamma = \xi_{\delta+2}\, \nabla\xi_5 - \xi_5\nabla\xi_{\delta+2} = (1-\xi_\delta)\,\nabla\xi_5 + \xi_5\nabla\xi_\delta \qquad (39)$$

are the zero-order curl-conforming functions of the two-dimensional simplexes defined by the triangular faces

$\xi_\delta = 0$ and $\xi_\gamma = 0$, respectively, with

$$\begin{cases} \nabla \times \boldsymbol{\Omega}_\delta = -2\,\boldsymbol{\ell}_{\gamma 5}/\mathcal{J} \\ \nabla \times \boldsymbol{\Omega}_\gamma = -2\,\boldsymbol{\ell}_{\delta 5}/\mathcal{J}. \end{cases} \tag{40}$$

At last, we clarify the order of the multiplicative polynomials (33) so as to prove the completeness of our bases as in the Appendix. $Q_k(\xi_5, \widetilde{\xi}_{\gamma\delta})$ is a polynomial of degree $3k$ of the $(\eta_\gamma, \eta_\delta, \xi_5)$ space whose highest degree term in ξ_5 is proportional to $(\xi_5 \eta_\gamma \eta_\delta)^k$. Its higher degree term in η_γ is proportional to $[\eta_\gamma (1 - \eta_\delta)(1 - \xi_5)]^k$, therefore proportional to ξ_γ^k on face $\xi_\delta = 0$. The highest degree term in η_δ is proportional to $[\eta_\delta(1 - \eta_\gamma)(1 - \xi_5)]^k$; that is, it is proportional to ξ_δ^k on the $\xi_\gamma = 0$ face. Similarly, one can show that the highest degree term of all the polynomials (33) obtained using the hierarchical indexing rule reported earlier is proportional to $(\eta_\gamma \eta_\delta \xi_5)^p$ and that we never obtain terms proportional to η_γ^α, η_δ^α, or ξ_5^α with $\alpha > p$.

Considering the expression (12), this is equivalent to saying that, for the maximum value assumed by the indexes i, j, and k, the component in $\nabla\xi_5$ of the functions (32) is of order $(p + 1)$ in η_1, η_2, and ξ_5. The $\nabla\xi_1$ component is of order p in η_1 and $(p + 1)$ in η_2; similarly, the $\nabla\xi_2$ component is of order p in η_2 and $(p + 1)$ in η_1. The same happens for the vector functions associated with the mixed edges considered in the previous subsections.

D. Degrees of Freedom

Not all the higher order *face-based* vector functions introduced so far are independent of each other. To form a p-th order base, we must discard the dependent functions and count the total number of degrees of freedom (DoFs). There are in all $8(p + 1)$ edge-based functions, since the pyramid has eight edges and all the edge-based functions are independent. Then, regarding the face-based functions, we observe that each lowest order vector function associated with the three edges that bound the *triangular* face $\xi_\gamma = 0$ generates a set of $p(p + 1)/2$ face-based functions

$$\boldsymbol{\Omega}_{i0k}^{\gamma 5} = H_{i0k}^{\gamma 5} \boldsymbol{\Omega}_{\gamma 5} \tag{41}$$

$$\boldsymbol{\Omega}_{i0k}^{\gamma,\gamma+1} = H_{i0k}^{\gamma,\gamma+1} \boldsymbol{\Omega}_{\gamma,\gamma+1} \tag{42}$$

$$\boldsymbol{\Omega}_{0jk}^{\gamma-1,\gamma} = H_{0jk}^{\gamma-1,\gamma} \boldsymbol{\Omega}_{\gamma-1,\gamma} \tag{43}$$

but one of these sets must be discarded, because, on a face, we have only two independent tangent vectors, as per the dependency relationship in Table I. So, for $p \geq 1$, on the $\xi_\gamma = 0$ face, we have a total of $p(p + 1)$ face-based functions. Similarly, since the *quadrilateral* face is bounded by four mixed-edges, we have four different subsets of vector functions based on face $\xi_5 = 0$. Two of these are dependent and must be discarded as per the dependency relationship in Table I. For example, the sets generated by the function $\boldsymbol{\Omega}_{35}$ and $\boldsymbol{\Omega}_{45}$ can be discarded. The remaining two sets

$$\boldsymbol{\Omega}_{0jk}^{15} = H_{0jk}^{15} \boldsymbol{\Omega}_{15} \tag{44}$$

$$\boldsymbol{\Omega}_{0jk}^{25} = H_{0jk}^{25} \boldsymbol{\Omega}_{25} \tag{45}$$

have in total $2p(p + 1)$ face-based functions, for $p \geq 1$. (Of course, one can use the face-based vector set $\boldsymbol{\Omega}^{35}$ instead of $\boldsymbol{\Omega}^{15}$, and/or the set $\boldsymbol{\Omega}^{45}$ instead of $\boldsymbol{\Omega}^{25}$.)
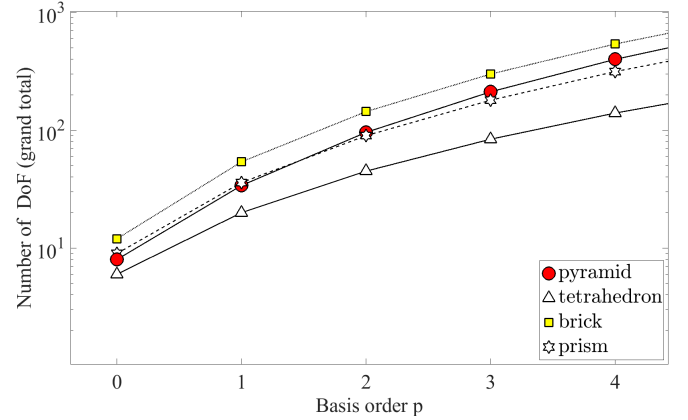

Fig. 2. Total number of DoFs for curl-conforming vector bases of order p on single, differently shaped canonical cells.

Finally, we have $3p^2(p + 1)$ bubble functions which are all independent. To summarize, the number of DoFs for curl-conforming bases of order p on a pyramid is determined as follows:

1) one component $\times (p + 1)$ DoFs $\times$ 8 edges $= 8(p + 1)$ edge DoF;
2) two components $\times p(p + 1)/2$ DoFs $\times$ four triangular faces $= 4p(p + 1)$ face DoF;
3) two components $\times p(p + 1)$ DoFs $\times$ one quadrilateral face $= 2p(p + 1)$ face DoF;
4) three components $\times p^2(p + 1)$ DoFs $\times$ one element $= 3p^2(p + 1)$ DoF interior to a pyramid

for a grand total of DoF per pyramid equal to

$$\text{DoF\#} = (p + 1)\big(8 + 6p + 3p^2\big) = 3\widetilde{p}^3 + 5\widetilde{p} \tag{46}$$

as obtained in [17] for $\widetilde{p} = p + 1$. The number of DoFs of the pyramid is always lower than that of the brick, while it remains higher than that of the triangular prism for $p \geq 2$ (see Fig. 2). Note that the pyramid and the brick have the same number of interior DoFs [6].

VI. NUMERICAL RESULTS

The principal concern of hierarchical bases tends to be the matrix conditioning arising from their use (see, for example, [6], paragraph 5.3.4, from page 242 onward). To establish that the rate of growth in CN for our new pyramidal bases is not substantially worse than that of the hierarchical bases for the other differently shaped cells (bricks, triangular-prisms, and tetrahedrons), we show in the following a couple of illustrative results obtained with rectilinear elements. We do this for the sake of brevity as our bases can also be used on curved pyramids appearing in hybrid meshes. To better assess (and then predict) the CN behavior, one should consider and study many hybrid meshes that use differently shaped elements.

Fig. 3 reports results for the individual element mass-matrix CNs for the hierarchical vector bases of different orders obtained by considering *rectilinear* cells with equal edges and of unitary length, computed with 3-D-integrals over the child cells. (Note that the CNs shown in Fig. 3 do not depend on the cell's edge length in the child space, since the unitary basis
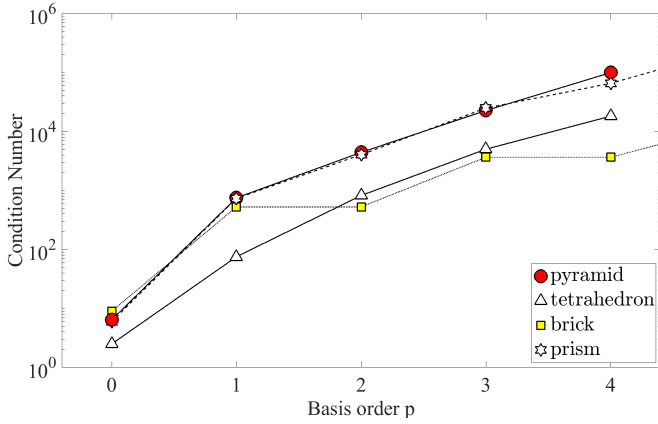
Fig. 3. Individual element mass-matrix CNs grow exponentially with the order of the hierarchical base in use. The figure shows results obtained by considering differently shaped rectilinear cells whose edges have the same unitary length. For $p \geq 1$, the CN associated with the pyramidal cell grows approximately as $50 \times 10^{1.3p}$ and, as shown, it is greater than that of the other equilateral elements of the same order reported in [6, Chap. 5].
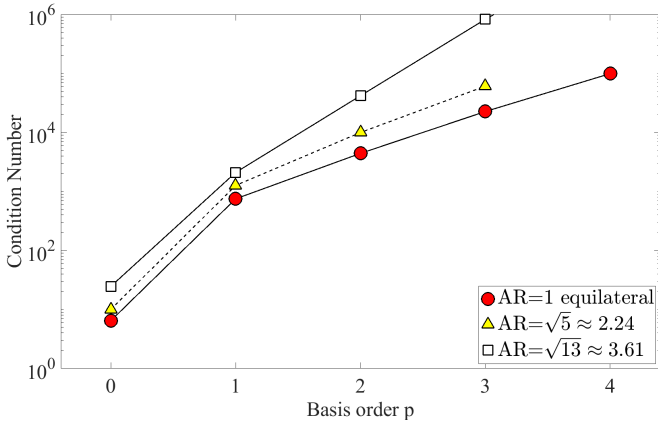

Fig. 4. Individual element mass-matrix CNs for the rectilinear pyramids shown in Fig. 5, with AR = 1 (equilateral), AR = $\sqrt{5}$, and AR = $\sqrt{13}$.

vectors and the Jacobian of the transformation from parent to child space are constant for the cells considered in Fig. 3.) The CNs of the pyramid shown in Fig. 3 are obtained by using for the triangular faces the basis functions associated with the triangle edges.

Fig. 4 compares the individual element mass-matrix CNs of the equilateral pyramid of Fig. 3 with those for pyramids obtained by moving one vertex of the base of the equilateral pyramid along its diagonal, doubling and tripling the length of this diagonal as depicted in Fig. 5. These pyramids have equal height and equal length for one of the diagonals of their base, but flat quadrilateral base of different shapes. The ratio between the longest and the shortest side of each cell, commonly known as aspect ratio (AR), is given in the captions of Figs. 4 and 5. Note that unlike the equilateral pyramid, the distorted pyramids considered in Fig. 4 do not have a constant Jacobian. In view of the (expected) results of Fig. 4, we recommend using cells with AR near unity and less than 3 when using bases of order higher than the first.

Table VII considers the first six resonant frequencies of a pyramidal cavity with the edges of equal length obtained by finding the eigenvalues of the discretized vector Helmholtz
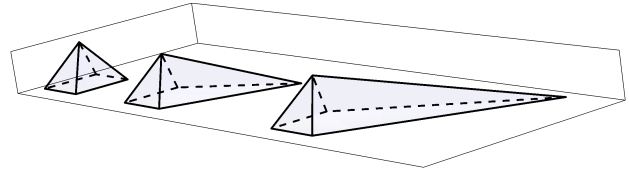

Fig. 5. Pyramids of different aspect ratios: AR = 1 (equilateral) in the left, AR = $\sqrt{5}$ in the center, and AR = $\sqrt{13}$ in the right. The Jacobian $\mathcal{J}$ of the transformation from the parent-to-child space is constant for an equilateral pyramid, while for distorted pyramids, it can vary within the cell. For example, we have $\mathcal{J} = K$ for the pyramid shown in the left, while $\mathcal{J} = K(1 + \eta_1 + \eta_2)$ for the pyramid shown in the center, and $\mathcal{J} = K(1 + 2\eta_1 + 2\eta_2)$ for the pyramid shown in the right.

TABLE VII

EQUILATERAL PYRAMID

	Meshing with 1 pyramid			
WN	$p = 3$	$p = 2$	$p = 1$	$p = 0$
5.780285 (1)	**5.776**	**5.81**	**6.03**	**6.32**
7.596937 (2)	**7.596**	**7.70**	**7.75**	**7.63**
9.264641 (2)	**9.319**	**9.93**	**10.10**	**9.26 (1)**
9.492400 (1)	**9.565**	**9.71**	**9.23**	
Max. Error	0.8%	7%	9%	10%
DoF	212	96	34	8
# of zero eigenvalues	76	36	14	4
CN	2.3×10^4	4.4×10^3	750	7
	Meshing with 4 tetrahedrons			
WN	$p = 3$	$p = 2$	$p = 1$	$p = 0$
5.780285 (1)	**5.778**	**5.82**	**5.64**	**6.32**
7.596937 (2)	**7.599**	**7.61**	**7.44**	**7.30**
9.264641 (2)	**9.329**	**9.30**	**9.48**	**8.00**
9.492400 (1)	**9.391**	**9.67**	**8.53**	**11.31**
Max. Error	1.1%	2%	9%	19%
DoF	244	123	50	13
CN	2.1×10^4	3.3×10^3	320	10

Results for a pyramid with edges of equal length. The first wavenumbers (WN) and their multiplicity (indicated in brackets) computed with bases of order $p = 3, 2, 1,$ and 0 are reported in red. The reference WN in the left column are obtained by meshing the pyramid with four identical tetrahedral cells of order $p = 6$, a problem with 1,015 DoF that leads to a mass-matrix CN=8.4×10^5. The results at top are obtained by meshing the pyramid with a single pyramidal element, those at the bottom are obtained by meshing the pyramid with four identical tetrahedral elements. For each order p, the Table also reports the maximum relative percentage error (Max. Error) found on the reported wavenumbers, the number of Degrees of Freedom (DoF), and the mass-matrix condition number (CN).

equation. Results obtained using a single pyramidal cell are compared with those obtained using *four* identical tetrahedral cells. These results not only demonstrate that our pyramid bases avoid spurious modes but are also capable of providing better results with fewer unknowns than that required by a tetrahedral cell-based model. To reduce the number of DoFs of the tetrahedral cell-based model, we also tried with a mesh formed by only two identical tetrahedral elements instead of

four (these results are not reported here), and we have seen that this heavily impacts on the symmetry of the cavity modes and leads to errors much higher than those reported in the lower part of Table VII.

VII. CONCLUSION

This article presents a general procedure to obtain higher order hierarchical curl-conforming vector basis functions for pyramidal elements. The functions ensure the continuity of the proper vector components across adjacent elements of equal order but different shapes. Properties of the vector basis functions are discussed in detail. The reported numerical examples show that higher order functions provide more accurate results than those obtainable with lower order elements.

APPENDIX
COMPLETENESS OF THE HIGH-ORDER VECTOR BASES

By using *homogeneous* multiplicative polynomials $\eta_1^\alpha \eta_2^\beta \xi_5^\gamma$, it follows from the last row of Table I that the following linear combinations of the curl-conforming bases yield complete vector polynomials of degree $p = (\alpha + \beta + \gamma)$ in three independent directions

$$\begin{bmatrix} \boldsymbol{\Omega}_{25} - \boldsymbol{\Omega}_{45} - \boldsymbol{\Omega}_{23} - \boldsymbol{\Omega}_{34} \\ \boldsymbol{\Omega}_{35} - \boldsymbol{\Omega}_{15} - \boldsymbol{\Omega}_{34} - \boldsymbol{\Omega}_{41} \\ \boldsymbol{\Omega}_{12} + \boldsymbol{\Omega}_{23} + \boldsymbol{\Omega}_{34} + \boldsymbol{\Omega}_{41} \end{bmatrix} \eta_1^\alpha \eta_2^\beta \xi_5^\gamma = \begin{bmatrix} \nabla\xi_1 \\ \nabla\xi_2 \\ \nabla\xi_5 \end{bmatrix} \eta_1^\alpha \eta_2^\beta \xi_5^\gamma. \quad (47)$$

In addition to that, we require that the set formed by the *curl* of the basis functions be complete to the order p; that is, all the vector polynomials of order $p+1$ with a *polynomial curl* must be a linear combination of our basis functions. Beware that our base does not model all vectors of order $p+1$, but only the physically acceptable ones, with nonzero polynomial curl. We therefore consider the *homogeneous* polynomials

$$\Psi^{(\alpha\beta\gamma)} = \eta_1^\alpha \eta_2^\beta \xi_5^\gamma (1 - \xi_5) \quad (48)$$

where we added the factor $(1 - \xi_5)$ to cancel the singularity in $\xi_5 = 1$ which would occur by calculating the gradient of $\eta_1^\alpha \eta_2^\beta \xi_5^\gamma$ for α or $\beta \neq 0$. For example, note that the linear combinations of the zeroth-order basis functions yield the high-order vectors

$$\begin{bmatrix} \boldsymbol{\Omega}_{35} + \boldsymbol{\Omega}_{45} \\ \boldsymbol{\Omega}_{25} - \boldsymbol{\Omega}_{45} \\ \boldsymbol{\Omega}_{35} - \boldsymbol{\Omega}_{15} \end{bmatrix} = \begin{bmatrix} \eta_1\nabla\xi_2 - \eta_2\nabla\xi_1 \\ \nabla\xi_1 + \eta_1\nabla\xi_5 \\ \nabla\xi_2 + \eta_2\nabla\xi_5 \end{bmatrix} \Psi^{(000)} \quad (49)$$

but none produce first-order, curl-free vectors such as $\xi_1\nabla\xi_1$, $\xi_2\nabla\xi_2$, and $\xi_5\nabla\xi_5$. It does not matter if the zero-order base is unable to produce "crystal-clear" terms like $\eta_1\Psi^{(000)}\nabla\xi_2 = \Psi^{(100)}\nabla\xi_2$; what really matters is that it must be able to produce $\nabla \times \Psi^{(100)}\nabla\xi_2$, as well as (see last row of Table I)

$$\frac{1}{2}\nabla \times \begin{bmatrix} \boldsymbol{\Omega}_{35} + \boldsymbol{\Omega}_{45} \\ \boldsymbol{\Omega}_{25} - \boldsymbol{\Omega}_{45} \end{bmatrix} = \nabla \times \Psi^{(1,0,0)} \begin{bmatrix} \nabla\xi_2 \\ \nabla\xi_5 \end{bmatrix} \quad (50)$$

$$\frac{1}{2}\nabla \times \begin{bmatrix} \boldsymbol{\Omega}_{35} + \boldsymbol{\Omega}_{45} \\ \boldsymbol{\Omega}_{35} - \boldsymbol{\Omega}_{15} \end{bmatrix} = \nabla \times \Psi^{(0,1,0)} \begin{bmatrix} -\nabla\xi_1 \\ \nabla\xi_5 \end{bmatrix}. \quad (51)$$

In essence, in addition to (47), it is necessary that the *curl* of some linear combinations of the vector basis functions

produces the curl of the terms reported in (52) and (53) unless a vector with zero curl

$$\begin{bmatrix} \nabla\xi_2 \\ \nabla\xi_5 \end{bmatrix} \Psi^{(\alpha+1,\beta,\gamma)} = \begin{bmatrix} \nabla\xi_2 \\ \nabla\xi_5 \end{bmatrix} \eta_1 \Psi^{(\alpha\beta\gamma)} \quad (52)$$

$$\begin{bmatrix} \nabla\xi_1 \\ \nabla\xi_5 \end{bmatrix} \Psi^{(\alpha,\beta+1,\gamma)} = \begin{bmatrix} \nabla\xi_1 \\ \nabla\xi_5 \end{bmatrix} \eta_2 \Psi^{(\alpha\beta\gamma)} \quad (53)$$

for $(\alpha + \beta + \gamma)$ varying between zero and p, and for α, β, and γ at most equal to p. Of course, once again, with these additions alone, we do not complete the base up to the order $(p + 1)$, because we discard linear combinations capable of producing

$$\Psi^{(p+1,0,0)}\nabla\xi_1, \ \Psi^{(0,p+1,0)}\nabla\xi_2, \ \Psi^{(0,0,p+1)}\nabla\xi_5. \quad (54)$$

The last term $\Psi^{(0,0,p+1)}\nabla\xi_5$ of (54) is discarded, because it is a curl-free term, while the first two terms are discarded, because their curl equals that of a vector function of order $p + 2$, as shown in (55), (56) (a p-order base does not need to model the curl of functions of order $p + 2$)

$$\nabla \times \left[\Psi^{(p+1,0,0)}\nabla\xi_1 \right] = -\frac{p}{p+2} \nabla \times \left[\Psi^{(p+2,0,0)}\nabla\xi_5 \right] \quad (55)$$

$$\nabla \times \left[\Psi^{(0,p+1,0)}\nabla\xi_2 \right] = -\frac{p}{p+2} \nabla \times \left[\Psi^{(0,p+2,0)}\nabla\xi_5 \right]. \quad (56)$$

Now, it is clear that the vectors (54) are discarded; let us prove completeness in the curl by using *inhomogeneous* polynomials. In this connection, we first observe that, with the exception of polynomials (54), any polynomial vector of order $(p + 1) = (\alpha + \beta + \gamma)$ can be expressed as the sum of a curl-free vector plus a vector which can be represented in terms of curl-conforming functions of order p

$$(1 + \alpha)\Psi^{(\alpha\beta\gamma)}\nabla\xi_1$$
$$= \nabla\left[\Psi^{(1,0,0)} \Psi^{(\alpha\beta\gamma)} \right]$$
$$\quad - \beta\Psi^{(\alpha+1,\beta-1,\gamma)}\nabla\xi_2 - (p-2)\Psi^{(\alpha+1,\beta,\gamma)}\nabla\xi_5$$
$$\quad - \gamma \Psi^{(\alpha+1,\beta,\gamma-1)}\nabla\xi_5 \quad (57)$$

$$(1 + \beta)\Psi^{(\alpha\beta\gamma)}\nabla\xi_2$$
$$= \nabla\left[\Psi^{(0,1,0)} \Psi^{(\alpha\beta\gamma)} \right]$$
$$\quad - \alpha\Psi^{(\alpha-1,\beta+1,\gamma)}\nabla\xi_1 - (p-2)\Psi^{(\alpha,\beta+1,\gamma)}\nabla\xi_5$$
$$\quad - \gamma \Psi^{(\alpha,\beta+1,\gamma-1)}\nabla\xi_5 \quad (58)$$

$$(2 - \alpha - \beta + \gamma)\Psi^{(\alpha\beta\gamma)}\nabla\xi_5$$
$$= \nabla\left[\Psi^{(0,0,1)} \Psi^{(\alpha\beta\gamma)} \right]$$
$$\quad - \alpha\Psi^{(\alpha-1,\beta,\gamma)}\nabla\xi_1 - \beta\Psi^{(\alpha,\beta-1,\gamma)}\nabla\xi_2$$
$$\quad - \gamma \Psi^{(\alpha,\beta,\gamma-1)}\nabla\xi_5 \quad (59)$$

with

$$p = \alpha + \beta + \gamma - 1 \geq 0$$
$$\alpha, \beta, \gamma \geq 0. \quad (60)$$

Notice that $\nabla[\Psi^{(1,0,0)} \Psi^{(\alpha\beta\gamma)}]$, $\nabla[\Psi^{(0,1,0)} \Psi^{(\alpha\beta\gamma)}]$, and $\nabla[\Psi^{(0,0,1)} \Psi^{(\alpha\beta\gamma)}]$ are the gradients of inhomogeneous polynomials and, because they are gradients, are curl-free. Taking the curl of both the sides of (57)–(59), one finds that the curl of any vector of order $(p + 1)$ (yielding a vector of order p) can always be expressed as a linear combination of the curl of curl-conforming bases of order p. Hence, the curl

of curl-conforming bases of order p is complete to order p within the space of vectors derivable from the curl of vectors of order $p + 1$. These bases appear in the inhomogeneous polynomial form in (57)–(59), but they are, of course, linear combinations of the polynomial bases defined in Section IV.

REFERENCES

[1] R. D. Graglia, D. R. Wilton, and A. F. Peterson, "Higher order interpolatory vector bases for computational electromagnetics," *IEEE Trans. Antennas Propag.*, vol. 45, no. 3, pp. 329–342, Mar. 1997.

[2] R. D. Graglia, D. R. Wilton, A. F. Peterson, and I.-L. Gheorma, "Higher order interpolatory vector bases on prism elements," *IEEE Trans. Antennas Propag.*, vol. 46, no. 3, pp. 442–450, Mar. 1998.

[3] R. D. Graglia, A. F. Peterson, and F. P. Andriulli, "Curl-conforming hierarchical vector bases for triangles and tetrahedra," *IEEE Trans. Antennas Propag.*, vol. 59, no. 3, pp. 950–959, Mar. 2011.

[4] R. D. Graglia and A. F. Peterson, "Hierarchical curl-conforming Nédélec elements for quadrilateral and brick cells," *IEEE Trans. Antennas Propag.*, vol. 59, no. 8, pp. 2766–2773, Aug. 2011.

[5] R. D. Graglia and A. F. Peterson, "Hierarchical curl-conforming Nédélec elements for triangular-prism cells," *IEEE Trans. Antennas Propag.*, vol. 60, no. 7, pp. 3314–3324, Jul. 2012.

[6] R. D. Graglia and A. F. Peterson, *Higher-Order Techniques in Computational Electromagnetics*. Edison, NJ, USA: SciTech Publishing, 2016.

[7] M. Salazar-Palma, T. K. Sarkar, L.-E. Garcia-Castillo, T. Roy, and A. Djordjevic, *Iterative and Self-Adaptive Finite-Elements in Electromagnetic Modeling*. Boston, MA, USA: Artech House, 1998.

[8] L. Demkowicz, *Computing With Hp-Adaptive Finite Elements*, vol. 1. Boca Raton, FL, USA: Chapman & Hall, 2007.

[9] L. Demkowicz, *Computing With Hp-Adaptive Finite Elements*, vol. 2. Boca Raton, FL, USA: Chapman & Hall, 2008.

[10] F. X. Zgainski, J. L. Coulomb, Y. Maréchal, F. Claeyssen, and X. Brunotte, "A new family of finite elements: The pyramidal elements," *IEEE Trans. Magn.*, vol. 32, no. 3, pp. 1393–1396, May 1996.

[11] R. D. Graglia and I.-L. Gheorma, "Higher order interpolatory vector bases on pyramidal elements," *IEEE Trans. Antennas Propag.*, vol. 47, no. 5, pp. 775–782, May 1999.

[12] J.-L. Coulomb, F.-X. Zgainski, and Y. Maréchal, "A pyramidal element to link hexahedral, prismatic and tetrahedral edge finite elements," *IEEE Trans. Magn.*, vol. 33, no. 2, pp. 1362–1365, Mar. 1997.

[13] V. Gradinaru and R. Hiptmair, "Whitney elements on pyramids," *Electron. Trans. Numer. Anal.*, vol. 8, pp. 154–168, Jan. 1999.

[14] M. Bergot, G. Cohen, and M. Duruflé, "Higher-order finite elements for hybrid meshes using new nodal pyramidal elements," *J. Sci. Comput.*, vol. 42, no. 3, pp. 345–381, Mar. 2010. [Online]. Available: https://hal.archives-ouvertes.fr/hal-00454261

[15] N. Nigam and J. Phillips, "Numerical integration for high order pyramidal finite elements," *ESAIM, Math. Model. Numer. Anal.*, vol. 46, p. 239, Mar. 2012.

[16] M. Bergot and M. Duruflé, "High-order optimal edge elements for pyramids, prisms and hexahedra," *J. Comput. Phys.*, vol. 232, no. 1, pp. 189–213, Jan. 2013.

[17] F. Fuentes, B. Keith, L. Demkowicz, and S. Nagaraj, "Orientation embedded high order shape functions for the exact sequence elements of all shapes," *Comput. Math. With Appl.*, vol. 70, no. 4, pp. 353–458, Aug. 2015.

[18] A. Gillette, "Serendipity and tensor product affine pyramid finite elements," *SMAI J. Comput. Math.*, vol. 2, pp. 215–228, Nov. 2016, doi: 10.5802/smai-jcm.14.

[19] N. Marais and D. B. Davidson, "Conforming arbitrary order hexahedral/tetrahedral hybrid discretisation," *Electron. Lett.*, vol. 44, no. 24, pp. 1384–1385, Dec. 2008.

[20] M. Abramowitz and I. Stegun, *Handbook of Mathematical Functions*. New York, NY, USA: Dover, 1968.

[21] I. S. Gradshteyn and I. M. Ryzhik, *Table of Integrals, Series, and Products*, 8th ed. New York, NY, USA: Academic, 2014.

[22] S. Zaglmayr, "High order finite element methods for electromagnetic field computation," Ph.D. Thesis, Inst. Numerische Math., Johannes Kepler Univ., Linz, Austria, Jul. 2006.

Roberto D. Graglia (Life Fellow, IEEE) received the Laurea degree *(summa cum laude)* in electronic engineering from the Politecnico di Torino, Turin, Italy, in 1979, and the Ph.D. degree in electrical engineering and computer science from the University of Illinois at Chicago, Chicago, IL, USA, in 1983.

From 1980 to 1981, he was a Research Engineer with the Centro Studi e Laboratori Telecomunicazioni (CSELT), Turin. He was a Teaching and Research Assistant with the University of Illinois at Chicago from 1981 to 1983 and later a Lecturer with the Politecnico di Torino from 1984 to 1991. From 1985 to 1992, he was a Researcher with the Italian National Research Council (CNR). In 1991 and 1993, he was an Associate Visiting Professor with the University of Illinois at Chicago. In 1992, he joined the Department of Electronics and Telecommunications, Politecnico di Torino, as an Associate Professor, where he has been a Professor of electrical engineering since 1999. He has authored or coauthored over 150 journal articles, book chapters, and conference proceedings. His areas of interests comprise numerical methods for high- and low-frequency electromagnetics, theoretical and computational aspects of scattering and interactions with complex media, waveguides, antennas, electromagnetic compatibility, and low-frequency phenomena.

Dr. Graglia was the recipient of the 2021 Harrington–Mittra Computational Electromagnetics Award. He was the President of the IEEE Antennas and Propagation Society in 2015. Since 1999, he has been the General Chairperson of the International Conference on Electromagnetics in Advanced Applications (ICEAA), and since 2011, he has been the General Chairperson of the IEEE-AP-S Topical Conference on Antennas and Propagation in Wireless Communications (IEEE-APWC). He was an Associate Editor of the IEEE TRANSACTIONS ON ANTENNAS AND PROPAGATION from 1995 to 1998, the IEEE TRANSACTIONS ON ELECTROMAGNETIC COMPATIBILITY from 1998 to 2000, and the IEEE ANTENNAS AND WIRELESS PROPAGATION LETTERS from 2002 to 2013, and he has been a member of the Editorial Board of Electromagnetics since 1997. He served the International Union of Radio Science (URSI) for the Triennial International Symposia on Electromagnetic Theory as an Organizer of the Special Session on Electromagnetic Compatibility (1998) and a co-organizer of the Special Session on Numerical Methods in 2004, and he was an Invited Convener at URSI General Assemblies for Special Sessions on Field and Waves in 1996, Electromagnetic Metrology in 1999, and Computational Electromagnetics in 1999. He was a Distinguished Lecturer of the IEEE Antennas and Propagation Society from 2009 to 2012.

Paolo Petrini (Member, IEEE) was born in Turin, Italy, on October 4, 1955. He received the Laurea degree *(summa cum laude)* in electronic engineering from the Politecnico di Torino, Turin, in 1979, with a graduation thesis on integrated optics, and the Ph.D. degree in electrical engineering from the Politecnico di Torino, in 2018.

From 1980 to 1981, he was a Research Engineer with CSELT, Italy, studying and measuring microwave subsystems for high-speed PSK radio links, and from 1981 to 1982, he was a Research Engineer with CERN (European Center for Nuclear Research, Geneva, Switzerland) involved in studying and measuring high-Q cavities for beam acceleration. From 1983 to 2012, he worked as a Registered Engineer working in RF-microwave and aerospace engineering, with customers among the most important Companies in Europe. Since 2012, he has been a Research Assistant with the Department of Electronics and Telecommunications, Politecnico di Torino. Since 2014, he has also been with the Department of Mechanical and Aerospace Engineering, Politecnico di Torino.